



Review

Bioactive Calcium Phosphate Coatings for Bone Implant Applications: A Review

Richard Drevet ^{1,*}, Joël Fauré ² and Hicham Benhayoune ²¹ Department of Physical Electronics, Masaryk University, Kotlářská 2, CZ-61137 Brno, Czech Republic² Institut de Thermique, Mécanique et Matériaux (ITheMM), EA 7548, Université de Reims Champagne-Ardenne (URCA), Bât.6, Moulin de la Housse, BP 1039 CEDEX 2, 51687 Reims, France; joel.fauré@univ-reims.fr (J.F.); hicham.benhayoune@univ-reims.fr (H.B.)

* Correspondence: drevet@mail.muni.cz or richarddrevet@yahoo.fr

Abstract: This review deals with the design of bioactive calcium phosphate coatings deposited on metallic substrates to produce bone implants. The bioceramic coating properties are used to create a strong bonding between the bone implants and the surrounding bone tissue. They provide a fast response after implantation and increase the lifespan of the implant in the body environment. The first part of the article describes the different compounds belonging to the calcium phosphate family and their main properties for applications in biomaterials science. The calcium-to-phosphorus atomic ratio (Ca/P)_{at.} and the solubility (K_s) of these compounds define their behavior in a physiological environment. Hydroxyapatite is the gold standard among calcium phosphate materials, but other chemical compositions/stoichiometries have also been studied for their interesting properties. The second part reviews the most common deposition processes to produce bioactive calcium phosphate coatings for bone implant applications. The last part describes key physicochemical properties of calcium phosphate coatings and their impact on the bioactivity and performance of bone implants in a physiological environment.

Keywords: biomaterials; coatings; calcium phosphates; hydroxyapatite; bone implant; biocompatibility; bioactivity; hard tissue repair



Citation: Drevet, R.; Fauré, J.; Benhayoune, H. Bioactive Calcium Phosphate Coatings for Bone Implant Applications: A Review. *Coatings* **2023**, *13*, 1091. <https://doi.org/10.3390/coatings13061091>

Academic Editor:
Eugenio Velasco-Ortega

Received: 11 May 2023
Revised: 9 June 2023
Accepted: 11 June 2023
Published: 13 June 2023



Copyright: © 2023 by the authors. Licensee MDPI, Basel, Switzerland. This article is an open access article distributed under the terms and conditions of the Creative Commons Attribution (CC BY) license (<https://creativecommons.org/licenses/by/4.0/>).

1. Introduction

The ageing of the world's population is creating an increasing clinical demand for skeletal repair [1–6]. In particular, orthopedic and dental surgeries require metallic bone implants made of titanium alloys [7–16], steels and iron-based alloys [17–21], or CoCr alloys [22–28]. The mechanical properties of these alloys are appropriate for load-bearing applications, and they are biocompatible with the body environment. According to the International Union of Pure and Applied Chemistry (IUPAC), biocompatibility is the *ability of a material to be in contact with a biological system without producing an adverse effect* [29–34]. However, surface modification of these metallic bone implants with a coating is necessary to make them bioactive in the body environment. Bioactivity is the *property of materials to develop a direct, adherent, and strong bonding with the bone tissue* [35–40]. Among the bioactive materials, calcium phosphates are most frequently used in industry and academic research. They are ceramic materials with a chemical composition akin to bone mineral, the inorganic component of our bones [41–47]. Inside the body, their bioactivity confers long-term performance on the metallic bone implant. They prevent bone anchorage failure and delay revision surgery [48–52]. Several methods can be used to produce calcium phosphate coatings on metallic bone implants including plasma spraying, magnetron sputtering, pulsed laser deposition, electrospray deposition, electrophoretic deposition, biomimetic deposition, a sol–gel process combined with dip or spin coating, electrodeposition, and hydrothermal synthesis [53]. Among them, plasma spraying is the main industrial process, extensively used since the 1970s to coat metallic bone implants [54]. Other deposition

processes have been developed for decades, and their advantages and drawbacks are well established today. The properties of a calcium phosphate coating depend on the process used to produce it and on the experimental conditions and deposition parameters as well. These are of great importance because the modification of coating properties is known to influence the surface bioactivity of the bone implant in a physiological environment.

2. Calcium Phosphates

Calcium phosphate bioceramics are materials made of calcium ions (Ca^{2+}) and phosphate ions (H_2PO_4^- , HPO_4^{2-} , or PO_4^{3-}). Several compounds belong to this family, with different stoichiometries and different phosphate species. They are specifically identified in biomaterials science by their calcium-to-phosphorus atomic ratio $(\text{Ca}/\text{P})_{\text{at}}$. (Table 1).

Table 1. Calcium phosphates described in the literature as coatings for bone implants.

$(\text{Ca}/\text{P})_{\text{at}}$	Calcium Phosphate	Abbreviation	Chemical Formulae	Solubility [$-\log K_s$]	References
2.00	tetracalcium phosphate	TTCP	$\text{Ca}_4(\text{PO}_4)_2\text{O}_2$	38.0–44.0	[55–57]
1.67	hydroxyapatite	HAP	$\text{Ca}_{10}(\text{PO}_4)_6\text{OH}_2$	116.8	[58–60]
1.50	α -tricalcium phosphate	α -TCP	$\alpha - \text{Ca}_3(\text{PO}_4)_2$	25.5	[61–63]
1.50	β -tricalcium phosphate	β -TCP	$\beta - \text{Ca}_3(\text{PO}_4)_2$	28.9	[64–66]
1.34–1.66	calcium-deficient apatite	Ca-def apatite	$\text{Ca}_{10-x}(\text{HPO}_4)_x(\text{PO}_4)_{6-x}(\text{OH})_{2-x}$ with $0 < x < 2$	85.1	[67–69]
1.33	octacalcium phosphate	OCP	$\text{Ca}_8(\text{HPO}_4)_2(\text{PO}_4)_4 \cdot 5\text{H}_2\text{O}$	96.6	[70–72]
1.00	calcium pyrophosphate	CPP	$\text{Ca}_2\text{P}_2\text{O}_7$	18.5	[73–75]
1.00	dicalcium phosphate anhydrous, also known as monetite	D CPA	CaHPO_4	6.9	[76–78]
1.00	dicalcium phosphate dihydrate, also known as brushite	D CPD	$\text{CaHPO}_4 \cdot 2\text{H}_2\text{O}$	6.6	[79–81]
0.50	monocalcium phosphate anhydrous	M CPA	$\text{Ca}(\text{H}_2\text{PO}_4)_2$	1.1	[82–84]
0.50	monocalcium phosphate monohydrate	M CPM	$\text{Ca}(\text{H}_2\text{PO}_4)_2 \cdot \text{H}_2\text{O}$	1.1	[85–87]

The stoichiometry of a calcium phosphate coating affects its solubility in a physiological environment, which is the first step involved in the bioactivity process after implantation (Figure 1).

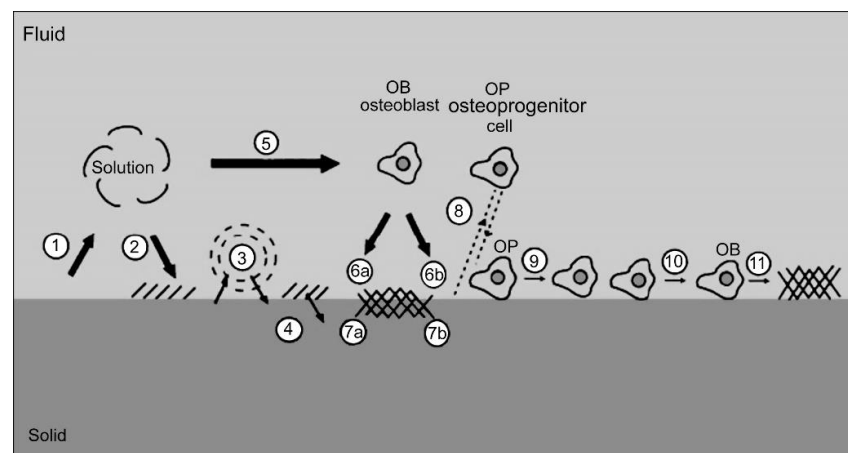


Figure 1. Schematic diagram of the events at the interface between a bioactive calcium phosphate coating (solid) and the surrounding physiological environment: (1) partial dissolution of the calcium phosphate coating; (2) precipitation from the solution;

(3) ion exchange and structural rearrangement at the bioceramic/tissue interface; (4) interdiffusion from the surface boundary layer into the bioceramics; (5) solution-mediated effects on cellular activity; (6) deposition of either the mineral phase (a) or the organic phase (b) without integration into the bioceramic surface; (7) deposition with integration into the bioceramics; (8) chemotaxis to the bioceramic surface; (9) cell attachment and proliferation; (10) cell differentiation; (11) extracellular matrix formation. Reprinted with permission from Ref. [88].

The partial dissolution of the calcium phosphate coating in contact with the physiological environment induces ionic releases. The local concentrations of calcium and phosphate ions increase up to supersaturation, which triggers the precipitation of biological apatite at the interface between the implant and the surrounding bone tissues [30,31,35–38]. After these first chemical steps, the biological steps start, involving bone cell attachment, proliferation, and differentiation. In the last step of the bioactivity process, the bone cells trigger the formation of the extracellular matrix (ECM), which is a three-dimensional network of macromolecules and minerals, such as collagen, enzymes, glycoproteins, and apatite [88–90]. The function of the extracellular matrix is to provide structural and biochemical support to the surrounding bone cells to promote their development [91]. Due to the bioactivity of the calcium phosphate coatings, bone-like apatite is formed at the interface between the bone implant and the bone tissue. This bone-like apatite layer is a direct, adherent, and strong bonding that results in the long-term stability of the bone implant inside the human body [92]. However, the success of the bioactivity process is related to several properties of the calcium phosphate coating and not only to the stoichiometry and solubility of the bioceramic material. The choice of the process and the experimental deposition conditions may influence many physicochemical properties of the calcium phosphate coating, and consequently the bioactivity process.

3. Deposition Methods

3.1. Plasma Spraying (PS)

Plasma spraying is the most widespread industrial process because it is remarkably efficient at producing large quantities of bioceramic coatings on metallic bone implants. However, a perfect reproducibility of the properties of the deposited coatings is impossible to achieve because of the highly nonlinear nature of the process [93,94].

In atmospheric plasma spraying (APS), calcium phosphate powder (generally hydroxyapatite) is injected into a plasma jet, the temperature of which is in the range of ten thousand degrees [95,96]. At this high temperature, the grains of powder are molten or partly molten. The plasma jet directs the molten droplets toward the bone implant surface, where the steps of spreading, accumulation, cooling, and solidification produce a coating (Figure 2).

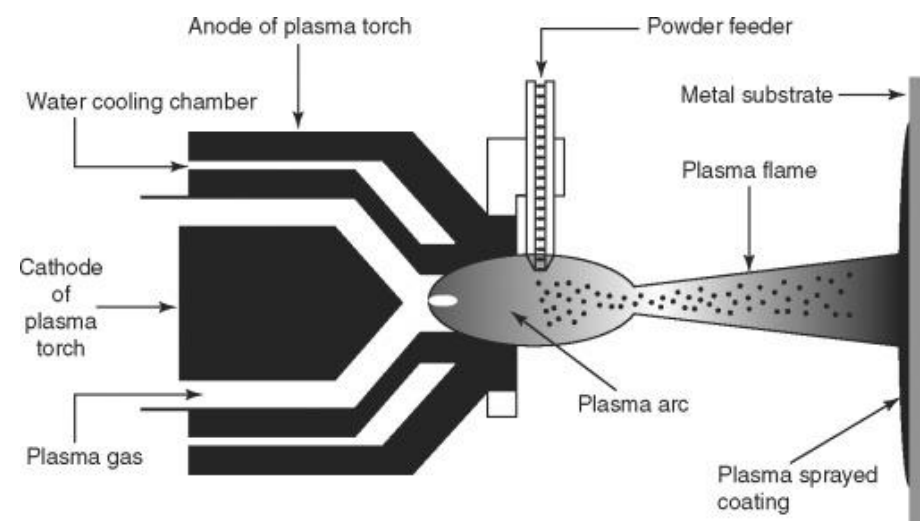
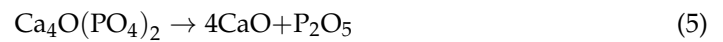
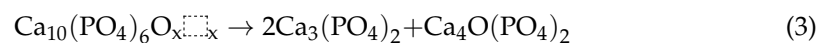
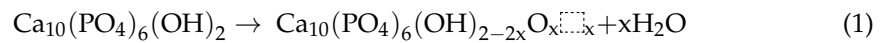


Figure 2. Schematic diagram of atmospheric plasma spray deposition of calcium phosphate coatings. Reprinted with permission from Ref. [97].

However, the high temperatures of the process give rise to several issues. The calcium phosphate particles melt incongruently, locally resulting in structural modifications, uncontrolled phase changes, and chemical decompositions. These modifications produce a coating, the physicochemical and biological properties of which differ from those of the initial powder [98–100]. The thermal decomposition of hydroxyapatite within a plasma is comprehensively described by Heimann's work on the following reactions [101]:



As a function of the experimental parameters, these five reactions may occur during plasma spray deposition, where O_x refers to lattice vacancies in the crystal structure of the calcium phosphate compound. The resulting bioceramic coating contains a mixture of oxyhydroxyapatite ($\text{Ca}_{10}(\text{PO}_4)_6(\text{OH})_{2-2x}\text{O}_x$), oxyapatite ($\text{Ca}_{10}(\text{PO}_4)_6\text{O}_x$), tricalcium phosphate ($\text{Ca}_3(\text{PO}_4)_2$), tetracalcium phosphate ($\text{Ca}_4\text{O}(\text{PO}_4)_2$), and calcium oxide (CaO) instead of pure hydroxyapatite as initially expected. All these additional phases affect the physicochemical properties of the coatings. Moreover, atmospheric plasma spray deposition produces coatings with residual stress, cracks, and interconnected porosity. These are caused by differences in the coefficients of thermal expansion of the substrate and coating, the imperfect melting of the particles, the insufficient flow of molten droplets in contact with the substrate, a rapid solidification rate, and poor interlayer bonding [102,103]. The rapid solidification induces a local melt-quenching of the particles that results in the amorphization of the bioceramics. The control of the chemical composition and structural properties of plasma-sprayed calcium phosphate coatings is difficult. They are made of several phases in several crystalline states, resulting in a highly heterogeneous bioactive behavior in a physiological environment. Nonetheless, the process is efficient in reaching industrial objectives, i.e., the production of large quantities of coatings at a low cost. The mechanical properties of the coatings are also satisfactory, especially their hardness and long-term stability in normal storage conditions. The adhesion to the metallic substrate is generally high enough, even though many research studies are still trying to find solutions to improve it [104]. Adhesion is a key property of industrial calcium phosphate coatings, the value of which is standardized for the biomedical market (see Section 4.6).

Atmospheric plasma spraying needs good flowability of the injected powder. This requirement limits the particle size of hydroxyapatite to coarse grains in the range of tens to hundreds of micrometers. Submicrometric powders cannot be directly used, because they tend to agglomerate readily due to high surface energy. The resulting flowability is not appropriate for plasma spray deposition. Suspension plasma spraying (SPS) and solution precursor plasma spraying (SPPS) are recent alternative processes that use a liquid feedstock injected into the plasma jet to produce sprayed calcium phosphate coatings [100]. Water or ethanol, or a mixture of both, is generally used. These two processes can produce nanostructured calcium phosphate coatings noted for their enhanced osseointegrative behavior [105,106].

Because the plasma spraying processes have advantages and drawbacks, the study of alternative deposition methods to produce calcium phosphate coatings for bone implant applications remains a major research topic for academic and industrial biomedical research.

3.2. Magnetron Sputtering (MS)

Magnetron sputtering of a calcium phosphate target is an alternative solution for producing bioactive calcium phosphate coatings on bone implants. Magnetron sputtering is a physical vapor deposition (PVD) process. A deposition chamber at room temperature is evacuated to a high vacuum to remove all potential contaminants. After the base pressure has been reached, a working gas is injected into the chamber, usually a noble gas such as argon. The resulting pressure is typically around 1 Pa. Plasma is then ignited from this noble gas by applying a high voltage between the cathode connected to the target and the anode connected to the deposition chamber as an electrical ground (Figure 3). The voltage necessary to start a discharge in a gas between two electrodes as a function of pressure and gap length is given by Paschen's law [107,108]. The process requires plasma ignition and a self-sustained discharge. Plasma contains high-energy ions that collide with the atoms of the target with enough energy to eject and transport them toward the surface of the bone implant to progressively form a coating [109].

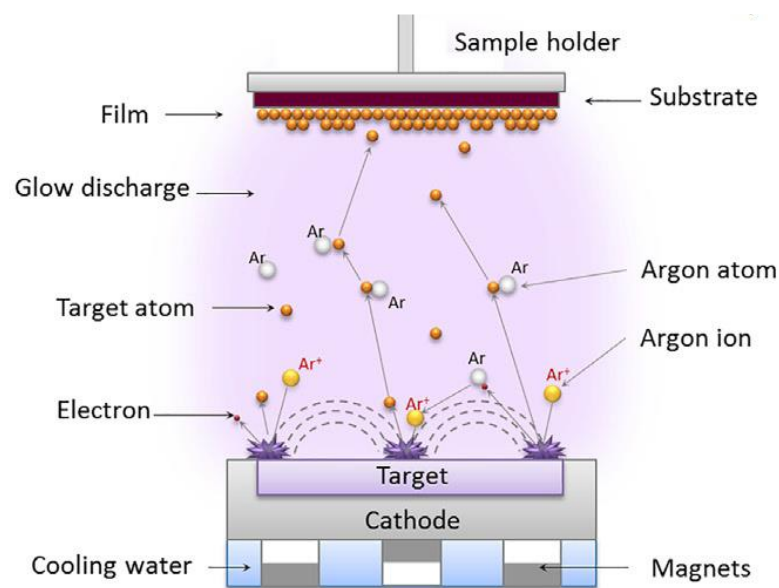


Figure 3. Schematic diagram of magnetron sputtering deposition of calcium phosphate coatings. Reprinted with permission from Ref. [109].

Direct current (DC) magnetron sputtering cannot be used to sputter insulating materials such as ceramics because of the charge accumulation within the target during the process. Pulsed-DC and radio frequency (RF) magnetron sputtering are alternative solutions for depositing insulating materials [110–112]. They produce dense, uniform, and adherent calcium phosphate coatings. However, the different elements of a multicomponent target have different sputtering behaviors. The elemental stoichiometry of the deposited coating usually differs from that of the target. The experimental parameters of the process can be used to modify some properties of the deposited calcium phosphate coatings such as stoichiometry, morphology, and structure, resulting in different bioactive behaviors [113–115].

3.3. Pulsed Laser Deposition (PLD)

Pulsed laser deposition is another PVD process carried out in a vacuum chamber [116–118]. The ablation of a calcium phosphate target hit by a high-power laser produces a plasma plume composed of ejected atoms, ions, and electrons (Figure 4). In contact with the substrate, the ejected material nucleates and grows to form a surface coating.

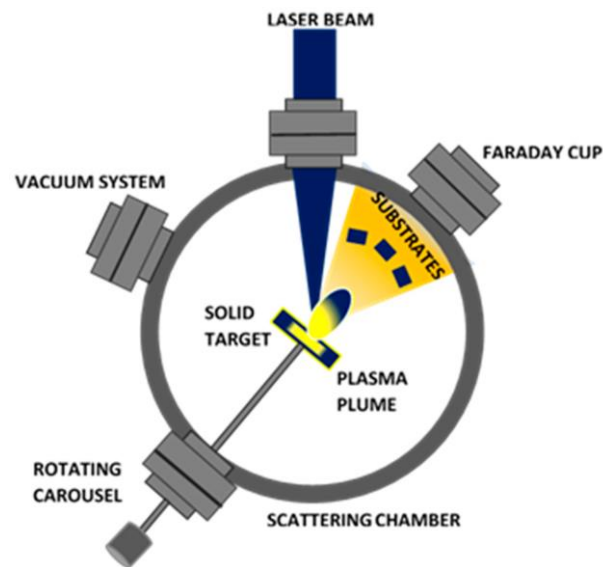


Figure 4. Schematic diagram of pulsed laser deposition of calcium phosphate coatings. Reprinted with permission from Ref. [119].

The efficiency of the process mainly depends on laser beam properties such as wavelength, energy density, fluence, and pulse width. Pulsed laser deposition produces uniform and adherent thin coatings. However, as observed for magnetron sputtering, the elemental stoichiometry of the target and that of the deposited coating are not identical. The physicochemical and biological properties of the coating are impacted by the experimental conditions of the process [120–122].

3.4. Electrospray Deposition (ESD)

Electrospray deposition requires a precursor solution containing calcium and phosphate ions, or a suspension of calcium phosphate particles. The solution is sprayed by using a syringe through a nozzle that is connected to a high voltage (Figure 5).

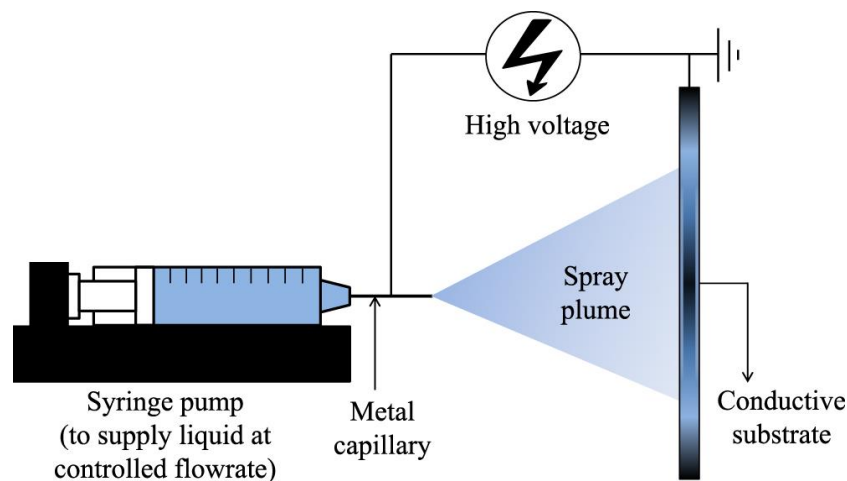


Figure 5. Schematic diagram of electrospray deposition of calcium phosphate coatings. Reprinted and adapted with permission from Ref. [123].

At the end of the capillary tube, the meniscus of the conducting solution becomes conical when charged (Taylor cone). Charged droplets are formed by the continuous breakup of the steady jet of solution leaving the tip of the nozzle. Solvent evaporation on the way toward the bone implant surface promotes the shrinkage of the charged droplets. In contact with the grounded and heated substrate, these very small droplets lose their surface charge and dry, progressively producing the bioactive coating (Figure 6).

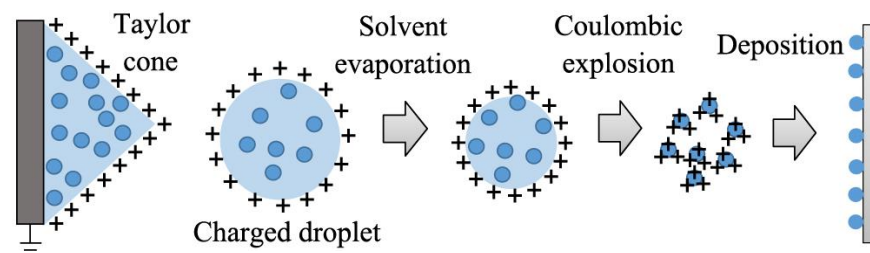


Figure 6. Schematic diagram of the droplets on their way from the tip of the needle to the substrate during the electro spray deposition process. Reprinted and adapted with permission from Ref. [123].

The morphology and structure of the coatings are impacted by properties of the solution such as conductivity and surface tension, and by electro spraying parameters such as voltage, flowrate, and distance between the needle tip and the substrate [124–128].

3.5. Electrophoretic Deposition (EPD)

Electrophoretic deposition occurs by means of the migration of calcium phosphate particles in a colloidal suspension [129–131]. In a solution, typically water or ethanol, the calcium phosphate particles carry a positive or negative surface charge due to electrostatic interactions with the ionic species of the solution. This surface charge induces the formation of a diffuse double layer containing anions and cations (Figure 7).

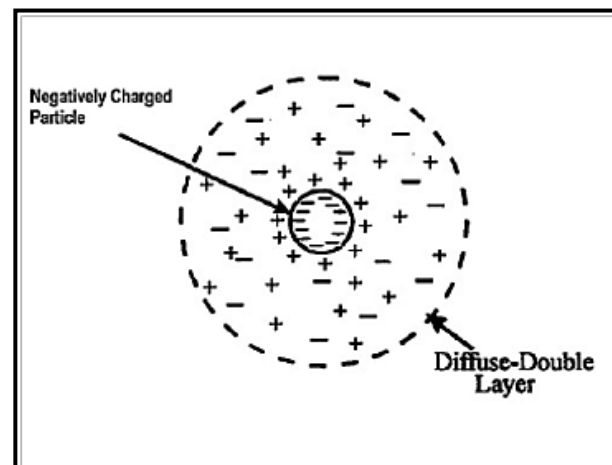


Figure 7. Model of the electric double layer of a negative particle in a solution. Reprinted with permission from Ref. [132].

The potential difference between the solution and the interface of the two layers is called zeta potential (ζ). This surface potential impacts the stability of colloidal dispersions by inducing electrostatic interactions between the particles of the suspension [132–138]. Thanks to the zeta potential, the particles can be accelerated under the influence of an electric field between two conductive electrodes connected to a generator. If the particles are positively charged, they move through the liquid toward the cathode (cathodic EPD in Figure 8a). If the particles are negatively charged, they move toward the anode (anodic EPD in Figure 8b).

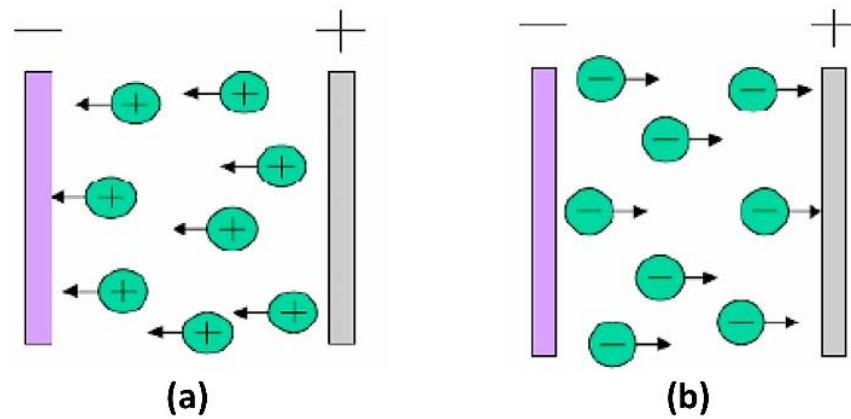


Figure 8. Schematic diagram of (a) cathodic EPD and (b) anodic EPD. Reprinted with permission from Ref. [132].

When a particle reaches the surface of an electrode, the size of the double layer is reduced (Figure 9a), promoting the progressive accumulation and coagulation of particles to form a calcium phosphate coating (Figure 9b).

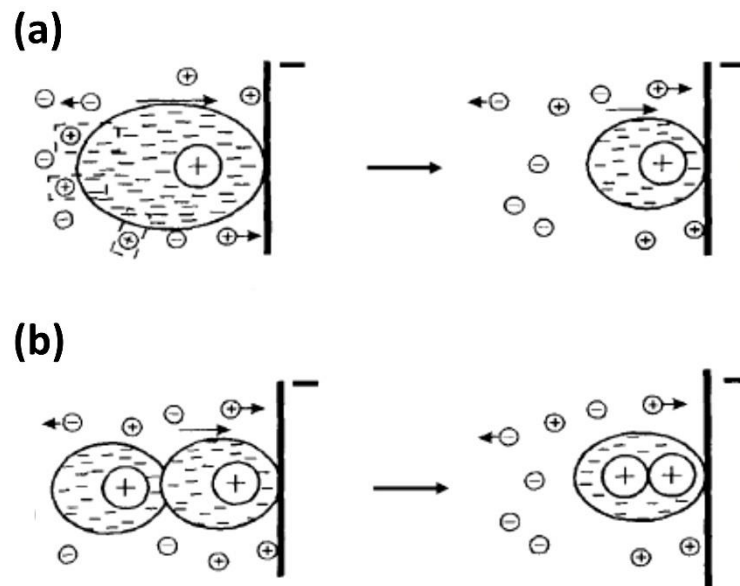


Figure 9. EPD coating formation model: (a) reduction in size of the double layer, (b) coagulation of particles. Reprinted with permission from Ref. [138].

The main parameters for the success of the EPD process are the pH and the stability of the suspension, the dielectric constant (ϵ) and the viscosity (η) of the solvent, the average particle size, the substrate conductivity, the voltage, the distance between the electrodes, and the deposition time. Post-deposition thermal annealing is required to evaporate the solvent and to improve the cohesive and adhesive properties of the coating [139,140].

3.6. Biomimetic Deposition

The surface of titanium and titanium alloys is naturally covered by a native oxide layer of TiO_2 produced by their reaction with oxygen in the air [141]. This surface layer is bioactive and promotes the slow deposition of a calcium phosphate coating during immersion in simulated body fluid (SBF) at 37°C , an acellular solution with pH and ion concentrations similar to those of human blood plasma (Table 2).

Table 2. Ion concentrations of blood plasma and SBF.

Ion	Concentrations (mM)	
	Blood Plasma (7.2 < pH < 7.4)	SBF (pH = 7.4)
Na ⁺	142.0	142.0
K ⁺	5.0	5.0
Mg ²⁺	1.5	1.5
Ca ²⁺	2.5	2.5
Cl ⁻	103.0	147.8
HCO ₃ ⁻	27.0	4.2
HPO ₄ ²⁻	1.0	1.0
SO ₄ ²⁻	0.5	0.5

These physiological conditions trigger the spontaneous nucleation and growth of apatite on the surface of the native TiO₂ layer. In the simulated body fluid, OH⁻ groups of the solution are adsorbed at the surface of TiO₂ and bond to titanium ions to produce Ti – OH groups. In slightly basic conditions, their deprotonation produces Ti – O⁻ groups that attract Ca²⁺ ions from the solution to form an amorphous surface layer of calcium titanate. Then, this positively charged layer attracts negatively charged phosphate ions to form a stable phase of amorphous calcium phosphate [142].

The biomimetic deposition process is very slow. Several days or weeks of immersion in SBF are necessary to produce a calcium phosphate coating a few micrometers thick. However, faster depositions have been observed for pretreated titanium surfaces [143]. Thermal annealing in air produces a thicker TiO₂ layer, the porosity of which accelerates the biomimetic deposition process. Another relevant pretreatment process is the immersion of titanium in a highly concentrated NaOH solution (typically 10 M) at 60 °C for 24 h. This alkaline treatment results in the formation of sodium titanate on the surface, which increases the reaction kinetics of the biomimetic deposition (Figure 10).

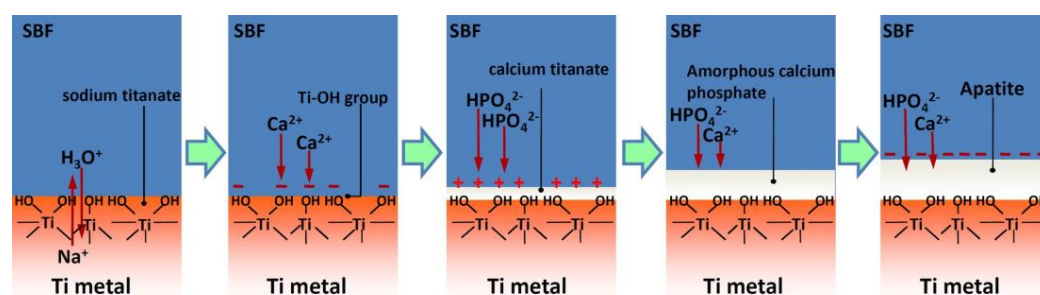


Figure 10. Mechanism of biomimetic apatite formation on NaOH treated titanium immersed in SBF. Reprinted with permission from Ref. [144].

3.7. Sol–Gel Process Combined with Dip or Spin Coating

Sol–gel is a low-temperature process that transforms an inorganic colloidal suspension (sol) into a three-dimensional network structure containing a liquid phase (gel). Calcium phosphate materials are produced by using calcium and phosphorus precursors [145–147]. Examples of calcium precursors described in the literature are calcium acetate monohydrate (Ca(CH₃COO)₂·H₂O), calcium nitrate tetrahydrate (Ca(NO₃)₂·4 H₂O), and calcium chloride (CaCl₂). Examples of phosphorus precursors are phosphoric acid (H₃PO₄), triethyl phosphite (P(OCH₂CH₃)₃), phosphorus pentoxide (P₂O₅), diammonium hydrogen orthophosphate ((NH₄)₂HPO₄), and trisodium phosphate (Na₃PO₄). They are dissolved separately in solvents that are typically water, ethanol, or a mixture of both. The dissolved precursors are then mixed dropwise and gently stirred. The two reactions

involved in the process are hydrolysis and condensation, the kinetics of which can be controlled by adjusting the pH value of the solution [148,149].

Thanks to the viscosity of the sol, the sol–gel process can be combined with dip coating or spin coating techniques to produce a surface coating (Figure 11). The dip coating technique involves the immersion and withdrawal of a substrate in the sol. The evaporation of the solvents in the air atmosphere during the drying step triggers the gelation process (polycondensation), which results in the formation of a calcium phosphate coating. The thickness of the coating depends mainly on the withdrawal speed and the viscosity of the sol.

The spin coating technique requires the deposition of the sol onto a substrate that is rotating around an axis perpendicular to the coated surface (Figure 11). The gelation step is also triggered by the evaporation of the solvent. The thickness of the coating depends mainly on the rotational speed and the viscosity of the sol.

The depositions are typically followed by thermal annealing at hundreds of degrees to densify the calcium phosphate coating and improve its mechanical properties.

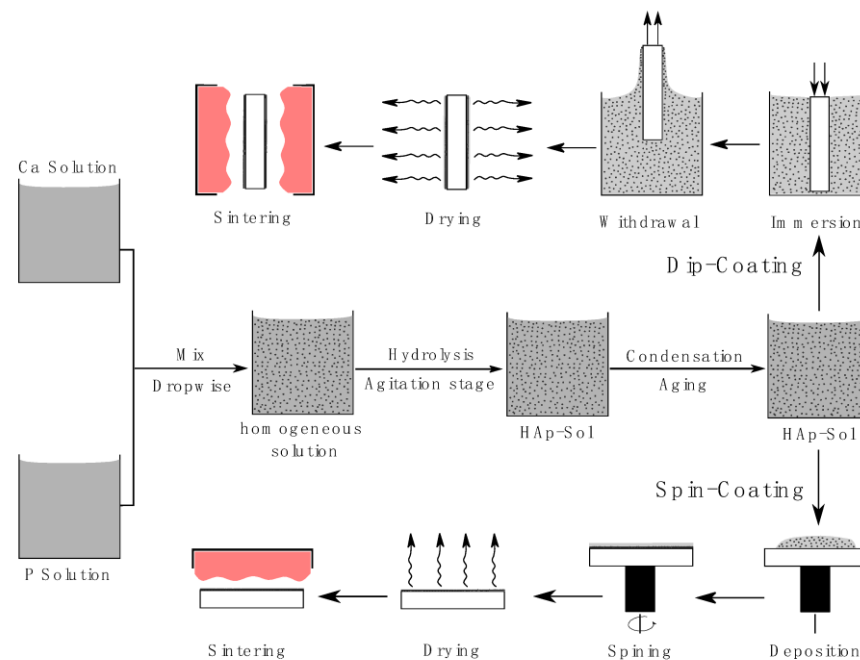


Figure 11. Steps of the sol–gel process to produce hydroxyapatite, and deposition by dip and spin coating. Reprinted with permission from Ref. [145].

3.8. Electrochemical Deposition (ECD)

The electrodeposition of calcium phosphate coatings requires two electrodes immersed in an electrolytic solution of calcium and phosphate ions. They are connected to a generator (Figure 12) [150–155].

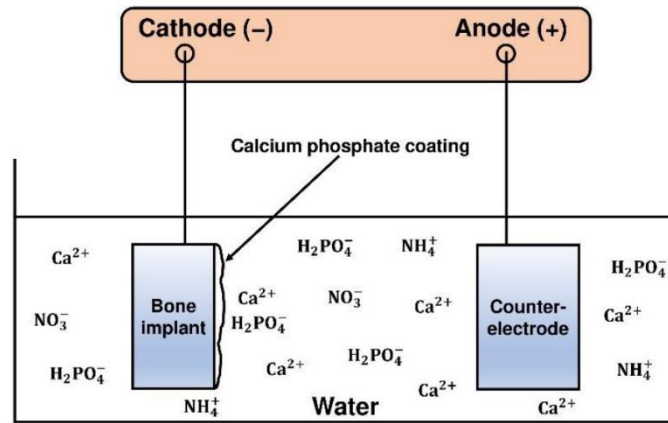


Figure 12. Schematic diagram of electrodeposition of calcium phosphate coatings. Reprinted with permission from Ref. [153].

Electrochemical reactions occur at both electrode–electrolyte interfaces. The reduction of water, the solvent of the solution, takes place at the cathode surface as follows:



If the solution is acidic, the reduction of protons may also occur at the cathode surface:



The resulting local pH variation triggers the precipitation of a calcium phosphate coating (Figure 13) [156–161].

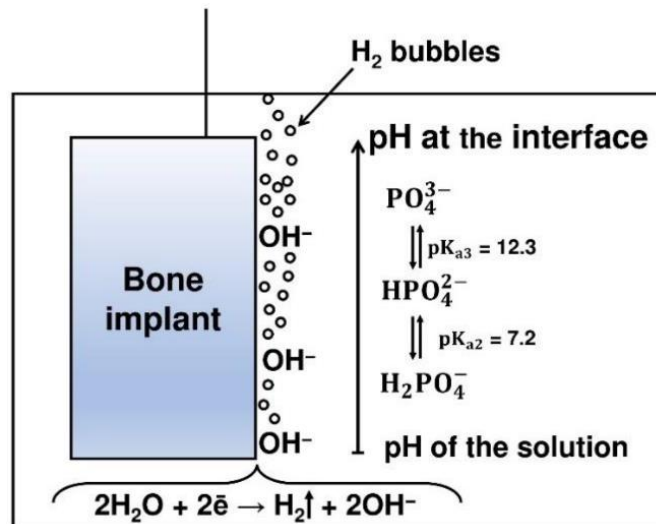


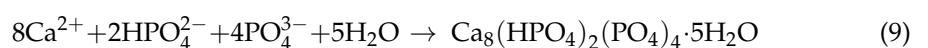
Figure 13. Schematic diagram of the cathode–electrolyte interface during electrodeposition. Reprinted with permission from Ref. [153].

The chemical composition and the stoichiometry of the precipitated coating depend on the pH value at the cathode, which is impacted by the process parameters. The following phases can be obtained:

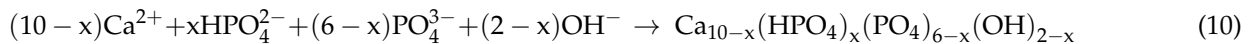
- dicalcium phosphate dihydrate (brushite):



- octacalcium phosphate:

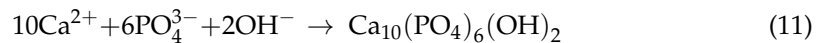


- calcium-deficient apatite:



with $0 < x < 2$

- hydroxyapatite:



The first experiments typically used direct current, but pulsed current electrodeposition has become more usual in the most recent years. The break times are used to remove the H₂ bubbles and to homogenize the electrolyte concentrations [162–166].

Another solution for reducing the amount of H₂ bubbles is the addition of hydrogen peroxide (H₂O₂) to the electrolyte solution [153]. Hydrogen peroxide is a strong oxidative reagent, the reduction of which produces hydroxide ions at the cathode according to the reaction (12):



However, the concentration of hydrogen peroxide in the electrolytic solution is limited because the overproduction of hydroxide ions prevents the deposition of the coating [153]. The optimization of the process showed that pulsed current electrodeposition from a 9 vol% H₂O₂ electrolyte solution produces stoichiometric hydroxyapatite (Ca/P = 1.67) according to the reaction (11).

In addition, the ionic substitution of the electrodeposited calcium phosphate coating can be easily obtained by modifying the electrolyte composition. Due to the low temperature of the process, the addition of organic components (polymers, proteins, drugs, etc.) is also possible to improve the biological and mechanical performances of the electrodeposited coating [167–169].

3.9. Hydrothermal Synthesis

Hydrothermal synthesis produces crystallized calcium phosphate coatings in a high-temperature solution under high pressure [170,171]. The aqueous solution contains calcium and phosphate ions. The process is carried out in an autoclave (Figure 14), typically at temperatures ranging from 100 °C to 350 °C and pressures up to 10⁷ Pa (100 bar). These extreme experimental conditions induce the precipitation of crystalline calcium phosphate crystals that nucleate and grow on the surface of bone implants. The crystallinity and the morphology of the coating are highly influenced by the pH of the solution and the temperature used during the process. As a function of the experimental conditions, different morphologies can be achieved, such as nanorods, microspheres, flakes, needles, hexagonal prisms, and hollow flowerlike structures [172].

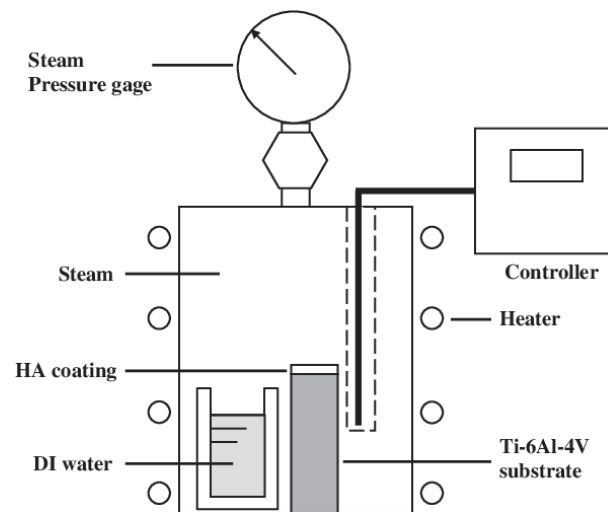


Figure 14. Schematic diagram of the autoclave for hydrothermal treatment. Reprinted with permission from Ref. [172].

The process can also be used as a complementary step to modify the crystallinity, morphology, porosity, and phase composition of calcium phosphate coatings deposited by other deposition methods, such as electrodeposition or plasma spraying. In fact, most of the previously described deposition methods produce calcium phosphates of low crystallinity. Dense calcium phosphate coatings with improved properties are described in the literature after post-deposition hydrothermal treatment under high temperature and high pressure [173,174]. Several works show the conversion of amorphous DCPD, OCP, or TCP into crystallized stoichiometric HAP by means of hydrothermal treatment.

4. Main Properties Impacting the Bioactivity of Calcium Phosphate Coatings

In addition to stoichiometry and solubility, several physicochemical properties impact the bioactivity of calcium phosphate coatings immersed in a physiological environment. Crystallinity, morphology, roughness, porosity, wettability, adhesion, and ionic substitution are the most important ones.

4.1. Crystallinity

The crystallinity of calcium phosphate coatings impacts their solubility in a physiological environment. The more crystallized the coating, the more stable it is in solution [175–177]. Crystallinity can be controlled by post-deposition thermal annealing. The international standard ISO 13779-2 recommends a degree of crystallinity higher than 45% for the biomedical market of bone implants [178]. However, as a function of the annealing temperature, several phases can form in addition to the calcium phosphate phases [179,180]. To maintain a low level of cytotoxicity, the quantity of secondary phases (for example CaO) in the calcium phosphate coatings should be below 5 wt.% [178]. The methods for determining the crystallinity of calcium phosphate coatings and the quantity of secondary phases are comprehensively described in the international standard ISO 13779-3 [181].

4.2. Morphology

The surface morphology of calcium phosphate coatings affects the bone cells' attachment, growth, proliferation, and differentiation [182,183]. As a function of the deposition process and the experimental conditions, the surface morphology of the coatings can change [184,185]. Regular surface morphologies are more efficient for bone cell attachment than irregular and sharp ones [186]. According to Cairns et al., they significantly promote the expression of growth factors involved in bone formation in comparison with sharp surfaces made of needles [187,188].

4.3. Roughness

Bioactivity is a surface phenomenon influenced by, among other factors, the roughness of materials. High roughness exceeding $2\ \mu\text{m}$ is not appropriate, because the long distances between valleys and peaks prevent the formation of the osteoblastic pseudopodia required for bone cell adhesion [189–191]. Calcium phosphate coatings with roughness values in the range of 0.5 to $1.5\ \mu\text{m}$ are generally described to be the most interesting for the promotion of bone cell activity [192–194].

4.4. Porosity

The porosity of calcium phosphate coatings has a significant impact on the bioactive behavior of bone implants in a physiological environment. Pores larger than one hundred micrometers (macroporosity) support the growth of bone tissues through the coating and improve the connection between newly formed bone cells. However, these large pores also strongly reduce the mechanical properties of the bioceramic coatings [195]. Smaller pores of a few tens of micrometers and below (microporosity) enhance protein adsorption, body fluid circulation, and the resorption rate of the coating [196].

4.5. Wettability

Surface wettability is a key property of calcium phosphate coatings because the bioactivity processes occur in a liquid medium. Contact angle (θ) measurements are used to quantify the wetting behavior of a drop of physiological solution deposited on the coating surface [197–199]. As a function of the contact angle value, the surface is qualified as hydrophilic or hydrophobic (Figure 15).

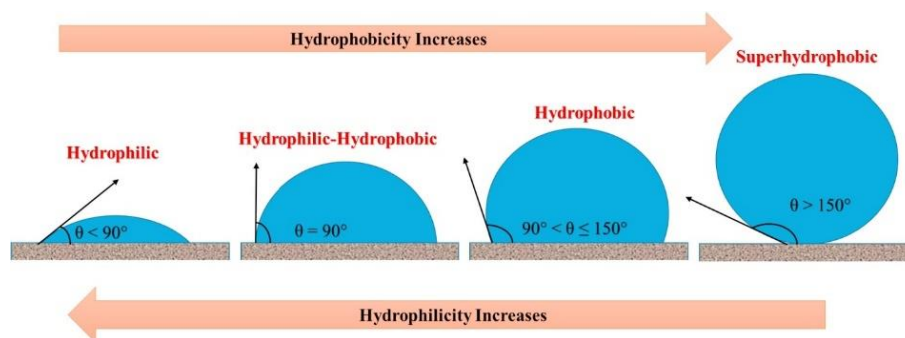


Figure 15. Surface wettability as a function of the contact angle measurement. Reprinted with permission from Ref. [200].

Biomaterials with hydrophilic surfaces are more effective in promoting chemical and biological interactions with the physiological environment [201,202].

4.6. Adhesion

The adhesion of calcium phosphate coatings is the main mechanical property required by the biomedical market [104,203–207]. The value of coatings is determined by performing tensile adhesion measurements according to the international standard ISO 13779-4 [208].

The measurement requires a Ti6Al4V cylinder (25 mm in diameter and 25 mm in height) with one surface coated with calcium phosphate. The coated surface is attached to another Ti6Al4V cylinder by adhesive glue (Figure 16a). The entire system is introduced into a standard tensile machine where an increasing load is applied (Figure 16b) until the separation of the coating is achieved by the breaking of the interface with the initially coated cylinder (Figure 16c). A cohesive failure inside the coating may also occur, but in this case, the measurement is not valid and must be repeated. A minimum of five measurements of adhesive failure is necessary to obtain an average adhesion value. The bone implant industry requires adhesion values higher than $15\ \text{MPa}$ [208].

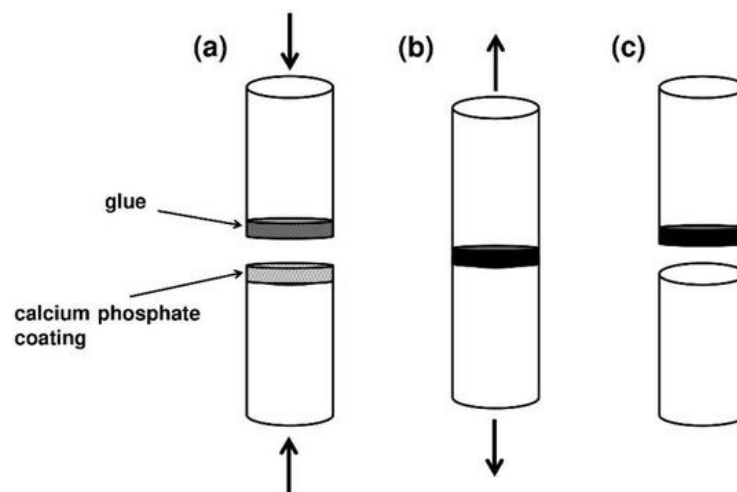


Figure 16. Schematic diagram of the standardized measurement of tensile adhesion. Reprinted with permission from Ref. [153].

This protocol is standardized for industrial applications, but several other methods can be used to determine the adhesion of calcium phosphate coatings, including the peel test, the scratch test, the ultrasonic test, and the laser shock adhesion test [104,209–213].

4.7. Ionic Substitution for Biological Enhancement

The bioactivity and biological properties of calcium phosphate coatings can be improved by means of ionic substitution [214–223]. The objective is to release the substituting ions in the physiological environment after implantation, taking advantage of the dissolution process (see Section 2). Several ionic substitutions have been described in the literature, using monovalent cations, divalent cations, trivalent cations, or anions. They are used to impart the various biological or chemical effects described in Table 3.

Table 3. Ions used as substituents in calcium phosphate coatings.

Ions	Biological/Chemical Effect	References
monovalent cations		
Ag ⁺	antibacterial activity	[224–226]
K ⁺	osteogenesis	[227–229]
Li ⁺	osteogenesis	[230–232]
Na ⁺	osteogenesis	[233–235]
divalent cations		
Co ²⁺	angiogenesis	[236–238]
Cu ²⁺	antibacterial activity	[239–241]
Mg ²⁺	osteogenesis	[242–244]
Mn ²⁺	osteogenesis	[245–247]
Sr ²⁺	osteogenesis	[248–251]
Zn ²⁺	osteogenesis/antibacterial/anti-inflammatory	[252–254]

Table 3. Cont.

Ions	Biological/Chemical Effect	References
trivalent cations		
Bi ³⁺	anticancer/antibacterial	[255–257]
Ce ³⁺	antibacterial	[258–261]
Er ³⁺	photoluminescence	[262–264]
Eu ³⁺	osteogenesis/photoluminescence	[265–267]
Fe ³⁺	osteogenesis/anticancer/antibacterial	[268–270]
Ga ³⁺	anticancer/antibacterial	[271–273]
Tb ³⁺	photoluminescence	[274,275]
anions		
Cl [−]	osteogenesis	[276–278]
CO ₃ ^{2−}	osteogenesis	[279–281]
F [−]	antibacterial	[282–284]
SeO ₃ ^{2−} /SeO ₄ ^{2−}	anticancer/antibacterial	[285–287]
SiO ₄ ^{4−}	osteogenesis	[288–290]

A few percent of these ions are generally used to produce substituted calcium phosphate coatings. Multi-substitution with several substituting ions is also described in the literature with the objective of cumulating its positive effects on the biological properties of bone implants [291–305].

5. Conclusions

This article reviewed the calcium phosphate compounds that are used as coatings to make the surface of metallic bone implants osseointegrative. The link between the stoichiometry, solubility, and bioactivity of calcium phosphate coatings was explained. The main processes used in industry and academic research to design calcium phosphate coatings were described. Historically, plasma spraying was the first industrial process, but interesting alternative methods were also developed and have been described herein. The stoichiometry and the physicochemical properties of the calcium phosphate coatings depend crucially on the deposition process and the experimental parameters used during coating deposition. The impact of coating properties on bioactivity has been briefly described. Finally, the ionic substitution of calcium phosphate coatings was reviewed from the literature, including the biological enhancements provided by ionic substitution.

Author Contributions: Conceptualization, R.D., J.F. and H.B.; methodology, R.D., J.F. and H.B.; validation, R.D., J.F. and H.B.; investigation, R.D., J.F. and H.B.; resources, R.D., J.F. and H.B.; writing—original draft preparation, R.D., J.F. and H.B.; writing—review and editing, R.D., J.F. and H.B. All authors have read and agreed to the published version of the manuscript.

Funding: This research received no external funding.

Institutional Review Board Statement: Not applicable.

Informed Consent Statement: Not applicable.

Data Availability Statement: Not applicable.

Conflicts of Interest: The authors declare no conflict of interest.

References

1. Available online: <https://www.who.int/news-room/fact-sheets/detail/ageing-and-health> (accessed on 10 May 2023).

2. Demontiero, O.; Vidal, C.; Duque, G. Aging and bone loss: New insights for the clinician. *Ther. Adv. Musculoskelet. Dis.* **2012**, *4*, 61–76. [[CrossRef](#)] [[PubMed](#)]
3. Gheno, R.; Cepparo, J.M.; Rosca, C.E.; Cotten, A. Musculoskeletal Disorders in the Elderly. *J. Clin. Imaging Sci.* **2012**, *2*, 39. [[CrossRef](#)] [[PubMed](#)]
4. U.S. Department of Health and Human Services. *Bone Health and Osteoporosis: A Report of the Surgeon General*; US Department of Health and Human Services, Office of the Surgeon General: Rockville, MD, USA, 2004. [[PubMed](#)]
5. Li, G.; Thabane, L.; Papaioannou, A.; Ioannidis, G.; Levine, M.A.H.; Adachi, J.D. An overview of osteoporosis and frailty in the elderly. *BMC Musculoskelet. Disord.* **2017**, *18*, 46. [[CrossRef](#)] [[PubMed](#)]
6. Bal, Z.; Kaito, T.; Korkusuz, F.; Yoshikawa, H. Bone regeneration with hydroxyapatite-based biomaterials. *Emergent Mater.* **2019**, *3*, 521–544. [[CrossRef](#)]
7. Farrakhov, R.; Melnichuk, O.; Parfenov, E.; Mukaeva, V.; Raab, A.; Sheremetyev, V.; Zhukova, Y.; Prokoshkin, S. Comparison of Biocompatible Coatings Produced by Plasma Electrolytic Oxidation on cp-Ti and Ti-Zr-Nb Superelastic Alloy. *Coatings* **2021**, *11*, 401. [[CrossRef](#)]
8. Ijaz, M.F.; Lailé, D.; Héraud, L.; Gordin, D.-M.; Castany, P.; Gloriant, T. Design of a novel superelastic Ti-23Hf-3Mo-4Sn biomedical alloy combining low modulus, high strength and large recovery strain. *Mater. Lett.* **2016**, *177*, 39–41. [[CrossRef](#)]
9. Sheremetyev, V.; Lukashevich, K.; Kreitchberg, A.; Kudryashova, A.; Tsaturyants, M.; Galkin, S.; Andreev, V.; Prokoshkin, S.; Brailovski, V. Optimization of a thermomechanical treatment of superelastic Ti-Zr-Nb alloys for the production of bar stock for orthopedic implants. *J. Alloys Compd.* **2022**, *928*, 167143. [[CrossRef](#)]
10. Lukashevich, K.; Sheremetyev, V.; Komissarov, A.; Cheverikin, V.; Andreev, V.; Prokoshkin, S.; Brailovski, V. Effect of Cooling and Annealing Conditions on the Microstructure, Mechanical and Superelastic Behavior of a Rotary Forged Ti-18Zr-15Nb (at. %) Bar Stock for Spinal Implants. *J. Funct. Biomater.* **2022**, *13*, 259. [[CrossRef](#)]
11. He, G.; Hagiwara, M. Ti alloy design strategy for biomedical applications. *Mater. Sci. Eng. C* **2006**, *26*, 14–19. [[CrossRef](#)]
12. Geetha, M.; Singh, A.K.; Asokamani, R.; Gogia, A.K. Ti based biomaterials, the ultimate choice for orthopaedic implants—A review. *Prog. Mater. Sci.* **2009**, *54*, 397–425. [[CrossRef](#)]
13. Chen, Q.; Thouas, G.A. Metallic implant biomaterials. *Mater. Sci. Eng. R Rep.* **2015**, *87*, 1–57. [[CrossRef](#)]
14. Sherif, E.-S.M.; Bahri, Y.A.; Alharbi, H.F.; Ijaz, M.F.; Alnaser, I.A. Influence of Tantalum Addition on the Corrosion Passivation of Titanium-Zirconium Alloy in Simulated Body Fluid. *Materials* **2022**, *15*, 8812. [[CrossRef](#)]
15. Andreucci, C.A.; Alshaya, A.; Fonseca, E.M.M.; Jorge, R.N. Proposal for a New Bioactive Kinetic Screw in an Implant, Using a Numerical Model. *Appl. Sci.* **2022**, *12*, 779. [[CrossRef](#)]
16. Jafari Chashmi, M.; Fathi, A.; Shirzad, M.; Jafari-Talookolaei, R.-A.; Bodaghi, M.; Rabiee, S.M. Design and Analysis of Porous Functionally Graded Femoral Prostheses with Improved Stress Shielding. *Designs* **2020**, *4*, 12. [[CrossRef](#)]
17. Drevet, R.; Zhukova, Y.; Malikova, P.; Dubinskiy, S.; Korotitskiy, A.; Pustov, Y.; Prokoshkin, S. Martensitic Transformations and Mechanical and Corrosion Properties of Fe-Mn-Si Alloys for Biodegradable Medical Implants. *Met. Mater. Trans. A* **2018**, *49*, 1006–1013. [[CrossRef](#)]
18. Drevet, R.; Zhukova, Y.; Kadirov, P.; Dubinskiy, S.; Kazakbiev, A.; Pustov, Y.; Prokoshkin, S. Tunable Corrosion Behavior of Calcium Phosphate Coated Fe-Mn-Si Alloys for Bone Implant Applications. *Met. Mater. Trans. A* **2018**, *49*, 6553–6560. [[CrossRef](#)]
19. Prokoshkin, S.; Pustov, Y.; Zhukova, Y.; Kadirov, P.; Dubinskiy, S.; Sheremetyev, V.; Karavaeva, M. Effect of Thermomechanical Treatment on Functional Properties of Biodegradable Fe-30Mn-5Si Shape Memory Alloy. *Met. Mater. Trans. A* **2021**, *52*, 2024–2032. [[CrossRef](#)]
20. Koumya, Y.; Salam, Y.A.; Khadiri, M.E.; Benzakour, J.; Romane, A.; Abouelfida, A.; Benyaich, A. Pitting corrosion behavior of SS-316L in simulated body fluid and electrochemically assisted deposition of hydroxyapatite coating. *Chem. Pap.* **2021**, *75*, 2667–2682. [[CrossRef](#)]
21. Trincă, L.C.; Burtan, L.; Mareci, D.; Fernández-Pérez, B.M.; Stoleriu, I.; Stanciu, T.; Stanciu, S.; Solcan, C.; Izquierdo, J.; Souto, R.M. Evaluation of in vitro corrosion resistance and in vivo osseointegration properties of a FeMnSiCa alloy as potential degradable implant biomaterial. *Mater. Sci. Eng. C* **2021**, *118*, 111436. [[CrossRef](#)]
22. Nkonta, D.V.T.; Simescu-Lazar, F.; Drevet, R.; Aaboubi, O.; Fauré, J.; Retraint, D.; Benhayoune, H. Influence of the surface mechanical attrition treatment (SMAT) on the corrosion behavior of Co28Cr6Mo alloy in Ringer’s solution. *J. Solid State Electrochem.* **2017**, *22*, 1091–1098. [[CrossRef](#)]
23. Chen, Y.; Li, Y.; Kurosu, S.; Yamanaka, K.; Tang, N.; Koizumi, Y.; Chiba, A. Effects of sigma phase and carbide on the wear behavior of CoCrMo alloys in Hanks’ solution. *Wear* **2013**, *310*, 51–62. [[CrossRef](#)]
24. Nkonta, D.T.; Drevet, R.; Fauré, J.; Benhayoune, H. Effect of surface mechanical attrition treatment on the microstructure of cobalt–chromium–molybdenum biomedical alloy. *Microsc. Res. Tech.* **2020**, *84*, 238–245. [[CrossRef](#)] [[PubMed](#)]
25. AlMangour, B.; Luqman, M.; Grzesiak, D.; Al-Harbi, H.; Ijaz, F. Effect of processing parameters on the microstructure and mechanical properties of Co–Cr–Mo alloy fabricated by selective laser melting. *Mater. Sci. Eng. A* **2020**, *792*, 139456. [[CrossRef](#)]
26. Yamanaka, K.; Mori, M.; Kurosu, S.; Matsumoto, H.; Chiba, A. Ultrafine Grain Refinement of Biomedical Co-29Cr-6Mo Alloy during Conventional Hot-Compression Deformation. *Met. Mater. Trans. A* **2009**, *40*, 1980–1994. [[CrossRef](#)]
27. Coşkun, M.I.; Karahan, I.H.; Yücel, Y.; Golden, T.D. Optimization of electrochemical step deposition for bioceramic hydroxyapatite coatings on CoCrMo implants. *Surf. Coat. Technol.* **2016**, *301*, 42–53. [[CrossRef](#)]

28. Coşkun, M.; Karahan, I.H.; Yücel, Y. Optimized Electrodeposition Concentrations for Hydroxyapatite Coatings on CoCrMo biomedical alloys by computational techniques. *Electrochim. Acta* **2014**, *150*, 46–54. [[CrossRef](#)]
29. Ghasemi-Mobarakeh, L.; Kolahreza, D.; Ramakrishna, S.; Williams, D. Key terminology in biomaterials and biocompatibility. *Curr. Opin. Biomed. Eng.* **2019**, *10*, 45–50. [[CrossRef](#)]
30. Williams, D. Revisiting the definition of biocompatibility. *Med. Device Technol.* **2003**, *14*, 10–13.
31. Williams, D.F. On the mechanisms of biocompatibility. *Biomaterials* **2008**, *29*, 2941–2953. [[CrossRef](#)]
32. Barrere, F.; Mahmood, T.A.; De Groot, K.; Van Blitterswijk, C.A. Advanced biomaterials for skeletal tissue regeneration: Instructive and smart functions. *Mater. Sci. Eng. R Rep.* **2008**, *59*, 38–71. [[CrossRef](#)]
33. Moniruzzaman, M.; O’Neal, C.; Bhuiyan, A.; Egan, P.F. Design and Mechanical Testing of 3D Printed Hierarchical Lattices Using Biocompatible Stereolithography. *Designs* **2020**, *4*, 22. [[CrossRef](#)]
34. Nuswantoro, N.F.; Lubis, M.A.R.; Juliadmi, D.; Mardawati, E.; Antov, P.; Kristak, L.; Hua, L.S. Bio-Based Adhesives for Orthopedic Applications: Sources, Preparation, Characterization, Challenges, and Future Perspectives. *Designs* **2022**, *6*, 96. [[CrossRef](#)]
35. Williams, D.F. Biocompatibility pathways and mechanisms for bioactive materials: The bioactivity zone. *Bioact. Mater.* **2021**, *10*, 306–322. [[CrossRef](#)]
36. Williams, D.F. On the nature of biomaterials. *Biomaterials* **2009**, *30*, 5897–5909. [[CrossRef](#)]
37. Cao, W.; Hench, L.L. Bioactive materials. *Ceram. Int.* **1996**, *22*, 493–507. [[CrossRef](#)]
38. Albrektsson, T.; Johansson, C. Osteoinduction, osteoconduction and osseointegration. *Eur. Spine J.* **2001**, *10*, S96–S101. [[CrossRef](#)]
39. Andreucci, C.A.; Fonseca, E.M.M.; Jorge, R.N. Bio-lubricant Properties Analysis of Drilling an Innovative Design of Bioactive Kinetic Screw into Bone. *Designs* **2023**, *7*, 21. [[CrossRef](#)]
40. Shaikh, M.S.; Fareed, M.A.; Zafar, M.S. Bioactive Glass Applications in Different Periodontal Lesions: A Narrative Review. *Coatings* **2023**, *13*, 716. [[CrossRef](#)]
41. Paital, S.R.; Dahotre, N.B. Calcium phosphate coatings for bio-implant applications: Materials, performance factors, and methodologies. *Mater. Sci. Eng. R Rep.* **2009**, *66*, 1–70. [[CrossRef](#)]
42. Dorozhkin, S.V. Calcium orthophosphate deposits: Preparation, properties and biomedical applications. *Mater. Sci. Eng. C* **2015**, *55*, 272–326. [[CrossRef](#)]
43. Dorozhkin, S.V. Bioceramics of calcium orthophosphates. *Biomaterials* **2010**, *31*, 1465–1485. [[CrossRef](#)] [[PubMed](#)]
44. LeGeros, R.Z. Calcium Phosphate-Based Osteoinductive Materials. *Chem. Rev.* **2008**, *108*, 4742–4753. [[CrossRef](#)] [[PubMed](#)]
45. Hench, L.L. Bioceramics. *J. Am. Ceram. Soc.* **1998**, *81*, 1705–1728. [[CrossRef](#)]
46. Navarrete-Segado, P.; Tourbin, M.; Grossin, D.; Frances, C. Tailoring hydroxyapatite suspensions by stirred bead milling. *Ceram. Int.* **2022**, *48*, 24953–24964. [[CrossRef](#)]
47. Dorozhkin, S.V. Calcium Orthophosphate (CaPO₄)-Based Bioceramics: Preparation, Properties, and Applications. *Coatings* **2022**, *12*, 1380. [[CrossRef](#)]
48. Surmenev, R.A.; Surmeneva, M.A.; Ivanova, A.A. Significance of calcium phosphate coatings for the enhancement of new bone osteogenesis—A review. *Acta Biomater.* **2014**, *10*, 557–579. [[CrossRef](#)]
49. Vallet-Regi, M.; González-Calbet, J.M. Calcium phosphates as substitution of bone tissues. *Prog. Solid State Chem.* **2004**, *32*, 1–31. [[CrossRef](#)]
50. Fiume, E.; Magnaterra, G.; Rahdar, A.; Verné, E.; Baino, F. Hydroxyapatite for Biomedical Applications: A Short Overview. *Ceramics* **2021**, *4*, 39. [[CrossRef](#)]
51. Jeong, J.; Kim, J.H.; Shim, J.H.; Hwang, N.S.; Heo, C.Y. Bioactive calcium phosphate materials and applications in bone regeneration. *Biomater. Res.* **2019**, *23*, 4. [[CrossRef](#)]
52. Lu, J.; Yu, H.; Chen, C. Biological properties of calcium phosphate biomaterials for bone repair: A review. *RSC Adv.* **2018**, *8*, 2015–2033. [[CrossRef](#)]
53. Drevet, R.; Benhayoune, H. Advanced Biomaterials and Coatings. *Coatings* **2022**, *12*, 965. [[CrossRef](#)]
54. McCabe, A.; Pickford, M.; Shawcross, J. The History, Technical Specifications and Efficacy of Plasma Spray Coatings Applied to Joint Replacement Prostheses. *Reconstr. Rev.* **2016**, *6*, 19–26. [[CrossRef](#)]
55. Moseke, C.; Gbureck, U. Tetracalcium phosphate: Synthesis, properties and biomedical applications. *Acta Biomater.* **2010**, *6*, 3815–3823. [[CrossRef](#)]
56. Qin, T.; Xu, Y. Fe-reinforced TTCP biocermet prepared via laser melting: Microstructure, mechanical properties and bioactivity. *Ceram. Int.* **2021**, *47*, 17652–17661. [[CrossRef](#)]
57. Mandal, S.; Meiningner, S.; Gbureck, U.; Basu, B. 3D powder printed tetracalcium phosphate scaffold with phytic acid binder: Fabrication, microstructure and in situ X-Ray tomography analysis of compressive failure. *J. Mater. Sci. Mater. Med.* **2018**, *29*, 29. [[CrossRef](#)]
58. LeGeros, R.Z. Properties of Osteoconductive Biomaterials: Calcium Phosphates. *Clin. Orthop. Relat. Res.* **2002**, *395*, 81–98. [[CrossRef](#)]
59. Hench, L.L. Bioceramics: From Concept to Clinic. *J. Am. Ceram. Soc.* **1991**, *74*, 1487–1510. [[CrossRef](#)]
60. Szczeń, A.; Hołysz, L.; Chibowski, E. Synthesis of hydroxyapatite for biomedical applications. *Adv. Colloid Interface Sci.* **2017**, *249*, 321–330. [[CrossRef](#)]
61. Carrodegua, R.G.; De Aza, S. α -Tricalcium phosphate: Synthesis, properties and biomedical applications. *Acta Biomater.* **2011**, *7*, 3536–3546. [[CrossRef](#)]

62. De Aza, P.N.; Luklinska, Z.B.; de Val, J.E.M.-S.; Calvo-Guirado, J.L. Biodegradation Process of α -Tricalcium Phosphate and α -Tricalcium Phosphate Solid Solution Bioceramics In Vivo: A Comparative Study. *Microsc. Microanal.* **2013**, *19*, 1350–1357. [[CrossRef](#)]
63. Kolmas, J.; Kafalak, A.; Zima, A.; Ślósarczyk, A. Alpha-tricalcium phosphate synthesized by two different routes: Structural and spectroscopic characterization. *Ceram. Int.* **2015**, *41*, 5727–5733. [[CrossRef](#)]
64. Bohner, M.; Santoni, B.L.G.; Döbelin, N. β -tricalcium phosphate for bone substitution: Synthesis and properties. *Acta Biomater.* **2020**, *113*, 23–41. [[CrossRef](#)] [[PubMed](#)]
65. Chaair, H.; Labjar, H.; Britel, O. Synthesis of β -tricalcium phosphate. *Morphologie* **2017**, *101*, 120–124. [[CrossRef](#)] [[PubMed](#)]
66. Drevet, R.; Fauré, J.; Sayen, S.; Marle-Spiess, M.; El Btaouri, H.; Benhayoune, H. Electrodeposition of biphasic calcium phosphate coatings with improved dissolution properties. *Mater. Chem. Phys.* **2019**, *236*, 121797. [[CrossRef](#)]
67. Drouet, C. Apatite Formation: Why It May Not Work as Planned, and How to Conclusively Identify Apatite Compounds. *BioMed Res. Int.* **2013**, *2013*, 490946. [[CrossRef](#)]
68. Valletregi, M.; Rodriguez-Lorenzo, L. Synthesis and characterisation of calcium deficient apatite. *Solid State Ion.* **1997**, *101–103*, 1279–1285. [[CrossRef](#)]
69. Hutchens, S.A.; Benson, R.S.; Evans, B.R.; O'Neill, H.; Rawn, C.J. Biomimetic synthesis of calcium-deficient hydroxyapatite in a natural hydrogel. *Biomaterials* **2006**, *27*, 4661–4670. [[CrossRef](#)]
70. Teterina, A.Y.; Smirnov, I.V.; Fadeeva, I.S.; Fadeev, R.S.; Smirnov, P.V.; Minaychev, V.V.; Kobayakova, M.I.; Fedotov, A.Y.; Barinov, S.M.; Komlev, V.S. Octacalcium Phosphate for Bone Tissue Engineering: Synthesis, Modification, and In Vitro Biocompatibility Assessment. *Int. J. Mol. Sci.* **2021**, *22*, 12747. [[CrossRef](#)]
71. Suzuki, O.; Hamai, R.; Sakai, S. The material design of octacalcium phosphate bone substitute: Increased dissolution and osteogenicity. *Acta Biomater.* **2023**, *158*, 1–11. [[CrossRef](#)]
72. Kovrlija, I.; Locs, J.; Loca, D. Octacalcium phosphate: Innovative vehicle for the local biologically active substance delivery in bone regeneration. *Acta Biomater.* **2021**, *135*, 27–47. [[CrossRef](#)]
73. Vasant, S.R.; Joshi, M.J. A review on calcium pyrophosphate and other related phosphate nano bio-materials and their applications. *Rev. Adv. Mater. Sci.* **2017**, *49*, 44–57.
74. Yan, Y.; Wolke, J.; De Ruijter, A.; Yubao, L.; Jansen, J. Growth behavior of rat bone marrow cells on RF magnetron sputtered hydroxyapatite and dicalcium pyrophosphate coatings. *J. Biomed. Mater. Res. Part A* **2006**, *78A*, 42–49. [[CrossRef](#)]
75. Golubchikov, D.; Safronova, T.V.; Nemygina, E.; Shatalova, T.B.; Tikhomirova, I.N.; Roslyakov, I.V.; Khayrutdinova, D.; Platonov, V.; Boytsova, O.; Kaimonov, M.; et al. Powder Synthesized from Aqueous Solution of Calcium Nitrate and Mixed-Anionic Solution of Orthophosphate and Silicate Anions for Bioceramics Production. *Coatings* **2023**, *13*, 374. [[CrossRef](#)]
76. Zhou, H.; Yang, L.; Gbureck, U.; Bhaduri, S.B.; Sikder, P. an important calcium phosphate compound—Its synthesis, properties and applications in orthopedics. *Acta Biomater.* **2021**, *127*, 41–55. [[CrossRef](#)]
77. da Silva, M.P.; Lima, J.; Soares, G.; Elias, C.; de Andrade, M.; Best, S.; Gibson, I. Transformation of monetite to hydroxyapatite in bioactive coatings on titanium. *Surf. Coat. Technol.* **2001**, *137*, 270–276. [[CrossRef](#)]
78. Ling, L.; Xin-Bo, X.; Jun, M.; Xin-Ye, N.; Xie-Rong, Z.; Sial, M.A.Z.G.; Dazhu, C. Post-hydrothermal treatment of hydrothermal electrodeposited CaHPO₄ on C/C composites in sodium silicate-containing solution at various temperatures. *Ceram. Int.* **2018**, *45*, 5894–5903. [[CrossRef](#)]
79. Tamimi, F.; Sheikh, Z.; Barralet, J. Dicalcium phosphate cements: Brushite and monetite. *Acta Biomater.* **2012**, *8*, 474–487. [[CrossRef](#)]
80. Türk, S.; Altınsoy, I.; Çelebiefte, G.; Ipek, M.; Özacar, M.; Bindal, C. Biomimetic coating of monophasic brushite on Ti6Al4V in new m-5xSBF. *Surf. Coat. Technol.* **2018**, *351*, 1–10. [[CrossRef](#)]
81. Lee, D.-W.; Shin, M.-C.; Kim, Y.-N.; Oh, J.-M. Brushite ceramic coatings for dental brace brackets fabricated via aerosol deposition. *Ceram. Int.* **2017**, *43*, 1044–1051. [[CrossRef](#)]
82. Su, Y.; Cockerill, I.; Zheng, Y.; Tang, L.; Qin, Y.-X.; Zhu, D. Biofunctionalization of metallic implants by calcium phosphate coatings. *Bioact. Mater.* **2019**, *4*, 196–206. [[CrossRef](#)]
83. Eliaz, N.; Metoki, N. Calcium Phosphate Bioceramics: A Review of Their History, Structure, Properties, Coating Technologies and Biomedical Applications. *Materials* **2017**, *10*, 334. [[CrossRef](#)] [[PubMed](#)]
84. Dorozhkin, S.V. Calcium orthophosphates (CaPO₄): Occurrence and properties. *Prog. Biomater.* **2015**, *5*, 9–70. [[CrossRef](#)] [[PubMed](#)]
85. Huan, Z.; Chang, J. Novel bioactive composite bone cements based on the β -tricalcium phosphate–monocalcium phosphate monohydrate composite cement system. *Acta Biomater.* **2008**, *5*, 1253–1264. [[CrossRef](#)] [[PubMed](#)]
86. Dorozhkin, S.V. A detailed history of calcium orthophosphates from 1770s till 1950. *Mater. Sci. Eng. C* **2013**, *33*, 3085–3110. [[CrossRef](#)]
87. Bermúdez, O.; Boltong, M.G.; Driessens, F.C.M.; Planell, J.A. Optimization of a calcium orthophosphate cement formulation occurring in the combination of monocalcium phosphate monohydrate with calcium oxide. *J. Mater. Sci. Mater. Med.* **1994**, *5*, 67–71. [[CrossRef](#)]
88. Ducheyne, P.; Qiu, Q. Bioactive ceramics: The effect of surface reactivity on bone formation and bone cell function. *Biomaterials* **1999**, *20*, 2287–2303. [[CrossRef](#)]
89. Kokubo, T.; Takadama, H. How useful is SBF in predicting in vivo bone bioactivity? *Biomaterials* **2006**, *27*, 2907–2915. [[CrossRef](#)]
90. Hoppe, A.; Güldal, N.S.; Boccaccini, A.R. A review of the biological response to ionic dissolution products from bioactive glasses and glass-ceramics. *Biomaterials* **2011**, *32*, 2757–2774. [[CrossRef](#)]

91. Bohner, M.; Lemaître, J. Can bioactivity be tested in vitro with SBF solution? *Biomaterials* **2009**, *30*, 2175–2179. [[CrossRef](#)]
92. Ho-Shui-Ling, A.; Bolander, J.; Rustom, L.E.; Johnson, A.W.; Luyten, F.P.; Picart, C. Bone regeneration strategies: Engineered scaffolds, bioactive molecules and stem cells current stage and future perspectives. *Biomaterials* **2018**, *180*, 143–162. [[CrossRef](#)]
93. Heimann, R.B. A Discussion on the Limits to Coating Reproducibility Based on Heat Transfer Instabilities. *J. Therm. Spray Technol.* **2019**, *28*, 327–332. [[CrossRef](#)]
94. Heimann, R.B.; Lehmann, H.D. *Bioceramic Coatings for Medical Implants: Trends and Techniques*; Wiley-VCH: Weinheim, Germany, 2015; pp. 253–308.
95. Sun, L.; Berndt, C.C.; Gross, K.A.; Kucuk, A. Material fundamentals and clinical performance of plasma-sprayed hydroxyapatite coatings: A review. *J. Biomed. Mater. Res.* **2001**, *58*, 570–592. [[CrossRef](#)]
96. Gross, K.A.; Walsh, W.; Swarts, E. Analysis of Retrieved Hydroxyapatite-Coated Hip Prostheses. *J. Therm. Spray Technol.* **2004**, *13*, 190–199. [[CrossRef](#)]
97. Wang, M. Composite coatings for implants and tissue engineering scaffolds. In *Biomedical Composites*, 1st ed.; Ambrosio, L., Ed.; Woodhead Publishing Series in Biomaterials: Cambridge, UK, 2010; Part 2, Chapter 6; pp. 127–177. [[CrossRef](#)]
98. Heimann, R.B. Plasma-Sprayed Hydroxylapatite-Based Coatings: Chemical, Mechanical, Microstructural, and Biomedical Properties. *J. Therm. Spray Technol.* **2016**, *25*, 827–850. [[CrossRef](#)]
99. Heimann, R.B. On the Self-Affine Fractal Geometry of Plasma-Sprayed Surfaces. *J. Therm. Spray Technol.* **2011**, *20*, 898–908. [[CrossRef](#)]
100. Chambard, M.; Marsan, O.; Charvillat, C.; Grossin, D.; Fort, P.; Rey, C.; Gitzhofer, F.; Bertrand, G. Effect of the deposition route on the microstructure of plasma-sprayed hydroxyapatite coatings. *Surf. Coat. Technol.* **2019**, *371*, 68–77. [[CrossRef](#)]
101. Heimann, R.B. Thermal spraying of biomaterials. *Surf. Coat. Technol.* **2006**, *201*, 2012–2019. [[CrossRef](#)]
102. Heimann, R.B. Structural Changes of Hydroxylapatite during Plasma Spraying: Raman and NMR Spectroscopy Results. *Coatings* **2021**, *11*, 987. [[CrossRef](#)]
103. Heimann, R.B. Functional plasma-sprayed hydroxylapatite coatings for medical application: Clinical performance requirements and key property enhancement. *J. Vac. Sci. Technol. A* **2021**, *39*, 050801. [[CrossRef](#)]
104. Mohseni, E.; Zalnezhad, E.; Bushroa, A. Comparative investigation on the adhesion of hydroxyapatite coating on Ti-6Al-4V implant: A review paper. *Int. J. Adhes. Adhes.* **2014**, *48*, 238–257. [[CrossRef](#)]
105. Pawlowski, L. Suspension and solution thermal spray coatings. *Surf. Coat. Technol.* **2009**, *203*, 2807–2829. [[CrossRef](#)]
106. Aruna, S.; Kulkarni, S.; Chakraborty, M.; Kumar, S.S.; Balaji, N.; Mandal, C. A comparative study on the synthesis and properties of suspension and solution precursor plasma sprayed hydroxyapatite coatings. *Ceram. Int.* **2017**, *43*, 9715–9722. [[CrossRef](#)]
107. Meek, J.M. A Theory of Spark Discharge. *Phys. Rev.* **1940**, *57*, 722–728. [[CrossRef](#)]
108. Boyle, W.S.; Kisliuk, P. Departure from Paschen's Law of Breakdown in Gases. *Phys. Rev.* **1955**, *97*, 255–259. [[CrossRef](#)]
109. Bonafos, C.; Khomenkhova, L.; Gourbilleau, F.; Talbot, E.; Slaoui, A.; Carrada, M.; Schamm-Chardon, S.; Dimitrakis, P.; Normand, P. Nano-composite MOx materials for NVMs. In *Metal Oxides for Non-Volatile Memory*, 1st ed.; Dimitrakis, P., Valov, I., Tappertzhofen, S., Eds.; Elsevier Science: Amsterdam, The Netherlands, 2022; Chapter 7; pp. 201–244.
110. Surmenev, R.A.; Ivanova, A.A.; Epple, M.; Pichugin, V.F.; Surmeneva, M.A. Physical principles of radio-frequency magnetron sputter deposition of calcium-phosphate-based coating with tailored properties. *Surf. Coat. Technol.* **2021**, *413*, 127098. [[CrossRef](#)]
111. Ivanova, A.; Surmeneva, M.; Tyurin, A.; Surmenev, R. Correlation between structural and mechanical properties of RF magnetron sputter deposited hydroxyapatite coating. *Mater. Charact.* **2018**, *142*, 261–269. [[CrossRef](#)]
112. Nelea, V.; Morosanu, C.; Iliescu, M.; Mihailescu, I. Microstructure and mechanical properties of hydroxyapatite thin films grown by RF magnetron sputtering. *Surf. Coat. Technol.* **2003**, *173*, 315–322. [[CrossRef](#)]
113. Safavi, M.S.; Surmeneva, M.A.; Surmenev, R.A.; Khalil-Allafi, J. RF-magnetron sputter deposited hydroxyapatite-based composite & multilayer coatings: A systematic review from mechanical, corrosion, and biological points of view. *Ceram. Int.* **2020**, *47*, 3031–3053. [[CrossRef](#)]
114. Chernozem, R.V.; Surmeneva, M.A.; Krause, B.; Baumbach, T.; Ignatov, V.P.; Tyurin, A.I.; Loza, K.; Epple, M.; Surmenev, R.A. Hybrid biocomposites based on titania nanotubes and a hydroxyapatite coating deposited by RF-magnetron sputtering: Surface topography, structure, and mechanical properties. *Appl. Surf. Sci.* **2017**, *426*, 229–237. [[CrossRef](#)]
115. Surmeneva, M.A.; Ivanova, A.A.; Tian, Q.; Pittman, R.; Jiang, W.; Lin, J.; Liu, H.H.; Surmenev, R.A. Bone marrow derived mesenchymal stem cell response to the RF magnetron sputter deposited hydroxyapatite coating on AZ91 magnesium alloy. *Mater. Chem. Phys.* **2018**, *221*, 89–98. [[CrossRef](#)]
116. Garcia-Sanz, F.J.; Mayor, M.B.; Arias, J.L.; Pou, J.; Leon, B.; Perez-Amor, M. Hydroxyapatite coatings: A comparative study between plasma-spray and pulsed laser deposition techniques. *J. Mater. Sci. Mater. Med.* **1997**, *8*, 861–865. [[CrossRef](#)]
117. Koch, C.; Johnson, S.; Kumar, D.; Jelinek, M.; Chrisey, D.; Doraiswamy, A.; Jin, C.; Narayan, R.; Mihailescu, I. Pulsed laser deposition of hydroxyapatite thin films. *Mater. Sci. Eng. C* **2007**, *27*, 484–494. [[CrossRef](#)]
118. Popescu-Pelin, G.; Sima, F.; Sima, L.; Mihailescu, C.; Luculescu, C.; Iordache, I.; Socol, M.; Socol, G. Hydroxyapatite thin films grown by pulsed laser deposition and matrix assisted pulsed laser evaporation: Comparative study. *Appl. Surf. Sci.* **2017**, *418*, 580–588. [[CrossRef](#)]
119. Cutroneo, M.; Havranek, V.; Flaks, J.; Malinsky, P.; Torrisi, L.; Silipigni, L.; Slepicka, P.; Fajstavr, D.; Mackova, A. Pulsed Laser Deposition and Laser-Induced Backward Transfer to Modify Polydimethylsiloxane. *Coatings* **2021**, *11*, 1521. [[CrossRef](#)]

120. Nishikawa, H.; Hasegawa, T.; Miyake, A.; Tashiro, Y.; Hashimoto, Y.; Blank, D.H.; Rijnders, G. Relationship between the Ca/P ratio of hydroxyapatite thin films and the spatial energy distribution of the ablation laser in pulsed laser deposition. *Mater. Lett.* **2016**, *165*, 95–98. [[CrossRef](#)]
121. González-Estrada, O.; Comas, A.P.; Ospina, R. Characterization of hydroxyapatite coatings produced by pulsed-laser deposition on additive manufacturing Ti6Al4V ELI. *Thin Solid Films* **2022**, *763*, 139592. [[CrossRef](#)]
122. Duta, L.; Popescu, A.C. Current Status on Pulsed Laser Deposition of Coatings from Animal-Origin Calcium Phosphate Sources. *Coatings* **2019**, *9*, 335. [[CrossRef](#)]
123. Saallah, S.; Lenggoro, I.W. Nanoparticles Carrying Biological Molecules: Recent Advances and Applications. *KONA Powder Part. J.* **2018**, *35*, 89–111. [[CrossRef](#)]
124. Leeuwenburgh, S.; Wolke, J.; Schoonman, J.; Jansen, J. Electrostatic spray deposition (ESD) of calcium phosphate coatings. *J. Biomed. Mater. Res. A* **2003**, *66*, 330–334. [[CrossRef](#)]
125. Leeuwenburgh, S.C.; Wolke, J.G.; Siebers, M.C.; Schoonman, J.; Jansen, J.A. In vitro and in vivo reactivity of porous, electrosprayed calcium phosphate coatings. *Biomaterials* **2006**, *27*, 3368–3378. [[CrossRef](#)]
126. Müller, V.; Pagnier, T.; Tadier, S.; Gremillard, L.; Jobbagy, M.; Djurado, E. Design of advanced one-step hydroxyapatite coatings for biomedical applications using the electrostatic spray deposition. *Appl. Surf. Sci.* **2020**, *541*, 148462. [[CrossRef](#)]
127. Huang, J.; Jayasinghe, S.; Best, S.M.; Edirisinghe, M.; Brooks, R.A.; Bonfield, W. Electrostatic spraying of a nano-hydroxyapatite suspension. *J. Mater. Sci.* **2004**, *39*, 1029–1032. [[CrossRef](#)]
128. Matsuura, T.; Maruyama, T. Calcium phosphate-polymer hybrid microparticles having functionalized surfaces prepared by a coaxially electrospray technique. *Colloids Surf. A Physicochem. Eng. Asp.* **2017**, *526*, 64–69. [[CrossRef](#)]
129. Boccaccini, A.R.; Keim, S.; Ma, R.; Li, Y.; Zhitomirsky, I. Electrophoretic deposition of biomaterials. *J. R. Soc. Interface* **2010**, *7* (Suppl. 5), S581–S613. [[CrossRef](#)]
130. Corni, I.; Ryan, M.P.; Boccaccini, A.R. Electrophoretic deposition: From traditional ceramics to nanotechnology. *J. Eur. Ceram. Soc.* **2008**, *28*, 1353–1367. [[CrossRef](#)]
131. Boccaccini, A.R.; Zhitomirsky, I. Application of electrophoretic and electrolytic deposition techniques in ceramics processing. *Curr. Opin. Solid State Mater. Sci.* **2002**, *6*, 251–260. [[CrossRef](#)]
132. Besra, L.; Liu, M. A review on fundamentals and applications of electrophoretic deposition (EPD). *Prog. Mater. Sci.* **2007**, *52*, 1–61. [[CrossRef](#)]
133. Drevet, R.; Ben Jaber, N.; Fauré, J.; Tara, A.; Larbi, A.B.C.; Benhayoune, H. Electrophoretic deposition (EPD) of nano-hydroxyapatite coatings with improved mechanical properties on prosthetic Ti6Al4V substrates. *Surf. Coat. Technol.* **2016**, *301*, 94–99. [[CrossRef](#)]
134. Azzouz, I.; Faure, J.; Khlifi, K.; Larbi, A.C.; Benhayoune, H. Electrophoretic Deposition of 45S5 Bioglass® Coatings on the Ti6Al4V Prosthetic Alloy with Improved Mechanical Properties. *Coatings* **2020**, *10*, 1192. [[CrossRef](#)]
135. Akhtar, M.A.; Hadzhiieva, Z.; Dlouhý, I.; Boccaccini, A.R. Electrophoretic Deposition and Characterization of Functional Coatings Based on an Antibacterial Gallium (III)-Chitosan Complex. *Coatings* **2020**, *10*, 483. [[CrossRef](#)]
136. Virk, R.S.; Rehman, M.A.U.; Munawar, M.A.; Schubert, D.W.; Goldmann, W.H.; Dusza, J.; Boccaccini, A.R. Curcumin-Containing Orthopedic Implant Coatings Deposited on Poly-Ether-Ether-Ketone/Bioactive Glass/Hexagonal Boron Nitride Layers by Electrophoretic Deposition. *Coatings* **2019**, *9*, 572. [[CrossRef](#)]
137. Bartmański, M.; Pawłowski, Ł.; Strugała, G.; Mielewczyk-Gryń, A.; Zieliński, A. Properties of Nanohydroxyapatite Coatings Doped with Nanocopper, Obtained by Electrophoretic Deposition on Ti13Zr13Nb Alloy. *Materials* **2019**, *12*, 3741. [[CrossRef](#)]
138. Sarkar, P.; Nicholson, P.S. Electrophoretic Deposition (EPD): Mechanisms, Kinetics, and Application to Ceramics. *J. Am. Ceram. Soc.* **1996**, *79*, 1987–2002. [[CrossRef](#)]
139. Kollath, V.O.; Chen, Q.; Closset, R.; Luyten, J.; Traina, K.; Mullens, S.; Boccaccini, A.; Cloots, R. AC vs. DC electrophoretic deposition of hydroxyapatite on titanium. *J. Eur. Ceram. Soc.* **2013**, *33*, 2715–2721. [[CrossRef](#)]
140. Azzouz, I.; Khlifi, K.; Faure, J.; Dhiflaoui, H.; Larbi, A.B.C.; Benhayoune, H. Mechanical behavior and corrosion resistance of sol-gel derived 45S5 bioactive glass coating on Ti6Al4V synthesized by electrophoretic deposition. *J. Mech. Behav. Biomed. Mater.* **2022**, *134*, 105352. [[CrossRef](#)]
141. Forsgren, J.; Svahn, F.; Jarmar, T.; Engqvist, H. Formation and adhesion of biomimetic hydroxyapatite deposited on titanium substrates. *Acta Biomater.* **2007**, *3*, 980–984. [[CrossRef](#)]
142. Kim, H.M.; Miyaji, F.; Kokubo, T.; Nakamura, T. Preparation of bioactive Ti and its alloys via simple chemical surface treatment. *J. Biomed. Mater. Res.* **1996**, *32*, 409–417. [[CrossRef](#)]
143. Pattanayak, D.K.; Yamaguchi, S.; Matsushita, T.; Kokubo, T. Nanostructured positively charged bioactive TiO₂ layer formed on Ti metal by NaOH, acid and heat treatments. *J. Mater. Sci. Mater. Med.* **2011**, *22*, 1803–1812. [[CrossRef](#)]
144. Kokubo, T.; Yamaguchi, S. Novel Bioactive Materials Derived by Bioglass: Glass-Ceramic A-W and Surface-Modified Ti Metal. *Int. J. Appl. Glas. Sci.* **2016**, *7*, 173–182. [[CrossRef](#)]
145. Jaafar, A.; Hecker, C.; Árki, P.; Joseph, Y. Sol-Gel Derived Hydroxyapatite Coatings for Titanium Implants: A Review. *Bioengineering* **2020**, *7*, 127. [[CrossRef](#)]
146. Jaafar, A.; Schimpf, C.; Mandel, M.; Hecker, C.; Rafaja, D.; Krüger, L.; Arki, P.; Joseph, Y. Sol-gel derived hydroxyapatite coating on titanium implants: Optimization of sol-gel process and engineering the interface. *J. Mater. Res.* **2022**, *37*, 2558–2570. [[CrossRef](#)]
147. Liu, D.-M.; Troczynski, T.; Tseng, W.J. Water-based sol-gel synthesis of hydroxyapatite: Process development. *Biomaterials* **2001**, *22*, 1721–1730. [[CrossRef](#)] [[PubMed](#)]

148. Asri, R.I.M.; Harun, W.S.W.; Hassan, M.A.; Ghani, S.A.C.; Buyong, Z. A review of hydroxyapatite-based coating techniques: Sol-gel and electrochemical depositions on biocompatible metals. *J. Mech. Behav. Biomed. Mater.* **2016**, *57*, 95–108. [[CrossRef](#)]
149. Choi, G.; Choi, A.H.; Evans, L.A.; Akyol, S.; Ben-Nissan, B. A review: Recent advances in sol-gel-derived hydroxyapatite nanocoatings for clinical applications. *J. Am. Ceram. Soc.* **2020**, *103*, 5442–5453. [[CrossRef](#)]
150. Shirkhazadeh, M. Bioactive calcium phosphate coatings prepared by electrodeposition. *J. Mater. Sci. Lett.* **1991**, *10*, 1415–1417. [[CrossRef](#)]
151. Shirkhazadeh, M. Calcium phosphate coatings prepared by electrocrystallization from aqueous electrolytes. *J. Mater. Sci. Mater. Med.* **1995**, *6*, 90–93. [[CrossRef](#)]
152. Drevet, R.; Benhayoune, H. Electrochemical Deposition of Calcium Phosphate Coatings on a Prosthetic Titanium Alloy Substrate. In *Calcium Phosphate: Structure, Synthesis, Properties and Applications*; Heimann, R.B., Ed.; Nova Science Publishers, Inc.: Hauppauge, NY, USA, 2012; pp. 231–252. ISBN 978-162257299-1.
153. Drevet, R.; Benhayoune, H. Electrodeposition of Calcium Phosphate Coatings on Metallic Substrates for Bone Implant Applications: A Review. *Coatings* **2022**, *12*, 539. [[CrossRef](#)]
154. Redepenning, J.; McIsaac, J.P. Electrocrystallization of brushite coatings on prosthetic alloys. *Chem. Mater.* **1990**, *2*, 625–627. [[CrossRef](#)]
155. Zhitomirsky, I. Cathodic electrodeposition of ceramic and organoceramic materials. Fundamental aspects. *Adv. Colloid Interface Sci.* **2002**, *97*, 279–317. [[CrossRef](#)]
156. Eliaz, N.; Eliyahu, M. Electrochemical processes of nucleation and growth of hydroxyapatite on titanium supported by real-time electrochemical atomic force microscopy. *J. Biomed. Mater. Res. Part A* **2007**, *80*, 621–634. [[CrossRef](#)]
157. Eliaz, N.; Sridhar, T.M. Electrocrystallization of Hydroxyapatite and Its Dependence on Solution Conditions. *Cryst. Growth Des.* **2008**, *8*, 3965–3977. [[CrossRef](#)]
158. Kuo, M.; Yen, S. The process of electrochemical deposited hydroxyapatite coatings on biomedical titanium at room temperature. *Mater. Sci. Eng. C* **2002**, *20*, 153–160. [[CrossRef](#)]
159. Zielinski, A.; Bartmanski, M. Electrodeposited Biocoatings, Their Properties and Fabrication Technologies: A Review. *Coatings* **2020**, *10*, 782. [[CrossRef](#)]
160. Lin, S.; LeGeros, R.Z.; LeGeros, J.P. Adherent octacalciumphosphate coating on titanium alloy using modulated electrochemical deposition method. *J. Biomed. Mater. Res. A* **2003**, *66*, 819–828. [[CrossRef](#)]
161. Furko, M.; Balázs, C. Calcium Phosphate Based Bioactive Ceramic Layers on Implant Materials Preparation, Properties, and Biological Performance. *Coatings* **2020**, *10*, 823. [[CrossRef](#)]
162. Drevet, R.; Lemelle, A.; Untereiner, V.; Manfait, M.; Sockalingum, G.; Benhayoune, H. Morphological modifications of electrodeposited calcium phosphate coatings under amino acids effect. *Appl. Surf. Sci.* **2013**, *268*, 343–348. [[CrossRef](#)]
163. Drevet, R.; Viteaux, A.; Maurin, J.C.; Benhayoune, H. Human osteoblast-like cells response to pulsed electrodeposited calcium phosphate coatings. *RSC Adv.* **2013**, *3*, 11148–11154. [[CrossRef](#)]
164. Vidal, E.; Buxadera-Palmero, J.; Pierre, C.; Manero, J.M.; Ginebra, M.-P.; Cazalbou, S.; Combes, C.; Rupérez, E.; Rodríguez, D. Single-step pulsed electrodeposition of calcium phosphate coatings on titanium for drug delivery. *Surf. Coat. Technol.* **2018**, *358*, 266–275. [[CrossRef](#)]
165. Jiménez-García, F.N.; Giraldo-Torres, L.; Restrepo-Parra, E. Electrochemically Deposited Calcium Phosphate Coatings Using a Potentiostat of In-house Design and Implementation. *Mater. Res.* **2021**, *24*, e20210098. [[CrossRef](#)]
166. Vidal, E.; Guillem-Martí, J.; Ginebra, M.-P.; Combes, C.; Rupérez, E.; Rodríguez, D. Multifunctional homogeneous calcium phosphate coatings: Toward antibacterial and cell adhesive titanium scaffolds. *Surf. Coat. Technol.* **2020**, *405*, 126557. [[CrossRef](#)]
167. Safavi, M.S.; Walsh, F.C.; Surmeneva, M.A.; Surmenev, R.A.; Khalil-Allafi, J. Electrodeposited Hydroxyapatite-Based Biocoatings: Recent Progress and Future Challenges. *Coatings* **2021**, *11*, 110. [[CrossRef](#)]
168. Gao, A.; Hang, R.; Bai, L.; Tang, B.; Chu, P.K. Electrochemical surface engineering of titanium-based alloys for biomedical application. *Electrochim. Acta* **2018**, *271*, 699–718. [[CrossRef](#)]
169. Ben Jaber, N.; Drevet, R.; Fauré, J.; Demangel, C.; Potiron, S.; Tara, A.; Larbi, A.B.C.; Benhayoune, H. A New Process for the Thermal Treatment of Calcium Phosphate Coatings Electrodeposited on Ti6Al4V Substrate. *Adv. Eng. Mater.* **2015**, *17*, 1608–1615. [[CrossRef](#)]
170. Suchanek, K.; Bartkowiak, A.; Gdowik, A.; Perzanowski, M.; Kaç, S.; Szaraniec, B.; Suchanek, M.; Marszałek, M. Crystalline hydroxyapatite coatings synthesized under hydrothermal conditions on modified titanium substrates. *Mater. Sci. Eng. C* **2015**, *51*, 57–63. [[CrossRef](#)]
171. Wen, S.; Liu, X.; Ding, J.; Liu, Y.; Lan, Z.; Zhang, Z.; Chen, G. Hydrothermal synthesis of hydroxyapatite coating on the surface of medical magnesium alloy and its corrosion resistance. *Prog. Nat. Sci.* **2021**, *31*, 324–333. [[CrossRef](#)]
172. Yang, C.-W.; Lui, T.-S.; Lee, T.-M.; Chang, E. Effect of Hydrothermal Treatment on Microstructural Feature and Bonding Strength of Plasma-Sprayed Hydroxyapatite on Ti-6Al-4V. *Mater. Trans.* **2004**, *45*, 2922–2929. [[CrossRef](#)]
173. Ling, L.; Cai, S.; Li, Q.; Sun, J.; Bao, X.; Xu, G. Recent advances in hydrothermal modification of calcium phosphorus coating on magnesium alloy. *J. Magnes. Alloy.* **2021**, *10*, 62–80. [[CrossRef](#)]
174. Yang, Y.; Wu, Q.; Wang, M.; Long, J.; Mao, Z.; Chen, X. Hydrothermal Synthesis of Hydroxyapatite with Different Morphologies: Influence of Supersaturation of the Reaction System. *Cryst. Growth Des.* **2014**, *14*, 4864–4871. [[CrossRef](#)]

175. Degli Esposti, L.; Markovic, S.; Ignjatovic, N.; Panseri, S.; Montesi, M.; Adamiano, A.; Fosca, M.; Rau, J.V.; Uskoković, V.; Iafisco, M. Thermal crystallization of amorphous calcium phosphate combined with citrate and fluoride doping: A novel route to produce hydroxyapatite bioceramics. *J. Mater. Chem. B* **2021**, *9*, 4832–4845. [[CrossRef](#)]
176. Gerk, S.A.; Golovanova, O.A.; Odazhiu, V.N. Structural, Morphological, and Resorption Properties of Carbonate Hydroxyapatite Prepared in the Presence of Glycine. *Inorg. Mater.* **2018**, *54*, 305–314. [[CrossRef](#)]
177. Hu, Q.; Tan, Z.; Liu, Y.; Tao, J.; Cai, Y.; Zhang, M.; Pan, H.; Xu, X.; Tang, R. Effect of crystallinity of calcium phosphate nanoparticles on adhesion, proliferation, and differentiation of bone marrow mesenchymal stem cells. *J. Mater. Chem.* **2007**, *17*, 4690–4698. [[CrossRef](#)]
178. ISO 13779-2; Implants for Surgery—Hydroxyapatite—Part 2: Thermally Sprayed Coatings of Hydroxyapatite. International Organization for Standardization: Geneva, Switzerland, 2018.
179. Raynaud, S.; Champion, E.; Bernache-Assollant, D. Calcium phosphate apatites with variable Ca/P atomic ratio II. Calcination and sintering. *Biomaterials* **2001**, *23*, 1073–1080. [[CrossRef](#)]
180. Destainville, A.; Champion, E.; Bernache-Assollant, D.; Laborde, E. Synthesis, characterization and thermal behavior of apatitic tricalcium phosphate. *Mater. Chem. Phys.* **2003**, *80*, 269–277. [[CrossRef](#)]
181. ISO 13779-3; Implants for Surgery—Hydroxyapatite—Part 3: Analyse Chimique et Caractérisation du Rapport de Cristallinité et de la Pureté de Phase. International Organization for Standardization: Geneva, Switzerland, 2018.
182. Katić, J.; Krivačić, S.; Petrović, Ž.; Mikić, D.; Marciuš, M. Titanium Implant Alloy Modified by Electrochemically Deposited Functional Bioactive Calcium Phosphate Coatings. *Coatings* **2023**, *13*, 640. [[CrossRef](#)]
183. Iwamoto, T.; Hieda, Y.; Kogai, Y. Effect of hydroxyapatite surface morphology on cell adhesion. *Mater. Sci. Eng. C* **2016**, *69*, 1263–1267. [[CrossRef](#)]
184. Drevet, R.; Fauré, J.; Benhayoune, H. Structural and morphological study of electrodeposited calcium phosphate materials submitted to thermal treatment. *Mater. Lett.* **2017**, *209*, 27–31. [[CrossRef](#)]
185. Liu, S.; Li, H.; Zhang, L.; Yin, X.; Guo, Y. In simulated body fluid performance of polymorphic apatite coatings synthesized by pulsed electrodeposition. *Mater. Sci. Eng. C* **2017**, *79*, 100–107. [[CrossRef](#)] [[PubMed](#)]
186. Lee, W.-K.; Lee, S.-M.; Kim, H.-M. Effect of surface morphology of calcium phosphate on osteoblast-like HOS cell responses. *J. Ind. Eng. Chem.* **2009**, *15*, 677–682. [[CrossRef](#)]
187. Cairns, M.; Meenan, B.; Burke, G.; Boyd, A. Influence of surface topography on osteoblast response to fibronectin coated calcium phosphate thin films. *Colloids Surf. B Biointerfaces* **2010**, *78*, 283–290. [[CrossRef](#)]
188. Pujari-Palmer, S.; Chen, S.; Rubino, S.; Weng, H.; Xia, W.; Engqvist, H.; Tang, L.; Ott, M.K. In vivo and in vitro evaluation of hydroxyapatite nanoparticle morphology on the acute inflammatory response. *Biomaterials* **2016**, *90*, 1–11. [[CrossRef](#)]
189. Chen, S.; Guo, Y.; Liu, R.; Wu, S.; Fang, J.; Huang, B.; Li, Z.; Chen, Z.; Chen, Z. Tuning surface properties of bone biomaterials to manipulate osteoblastic cell adhesion and the signaling pathways for the enhancement of early osseointegration. *Colloids Surf. B Biointerfaces* **2018**, *164*, 58–69. [[CrossRef](#)] [[PubMed](#)]
190. Khlusov, I.A.; Dekhtyar, Y.; Sharkeev, Y.P.; Pichugin, V.F.; Khlusova, M.Y.; Polyaka, N.; Tyulkin, F.; Vendinya, V.; Legostaeva, E.V.; Litvinova, L.S.; et al. Nanoscale Electrical Potential and Roughness of a Calcium Phosphate Surface Promotes the Osteogenic Phenotype of Stromal Cells. *Materials* **2018**, *11*, 978. [[CrossRef](#)]
191. Deligianni, D.D.; Katsala, N.D.; Koutsoukos, P.G.; Missirlis, Y.F. Effect of surface roughness of hydroxyapatite on human bone marrow cell adhesion, proliferation, differentiation and detachment strength. *Biomaterials* **2000**, *22*, 87–96. [[CrossRef](#)] [[PubMed](#)]
192. Anselme, K.; Bigerelle, M. On the relation between surface roughness of metallic substrates and adhesion of human primary bone cells. *Scanning* **2012**, *36*, 11–20. [[CrossRef](#)] [[PubMed](#)]
193. Giljean, S.; Bigerelle, M.; Anselme, K. Roughness statistical influence on cell adhesion using profilometry and multiscale analysis. *Scanning* **2012**, *36*, 2–10. [[CrossRef](#)]
194. Adeleke, S.; Ramesh, S.; Bushroa, A.; Ching, Y.; Sopyan, I.; Maleque, M.; Krishnasamy, S.; Chandran, H.; Misran, H.; Sutharsini, U. The properties of hydroxyapatite ceramic coatings produced by plasma electrolytic oxidation. *Ceram. Int.* **2018**, *44*, 1802–1811. [[CrossRef](#)]
195. Pecqueux, F.; Tancret, F.; Payraudeau, N.; Bouler, J. Influence of microporosity and macroporosity on the mechanical properties of biphasic calcium phosphate bioceramics: Modelling and experiment. *J. Eur. Ceram. Soc.* **2010**, *30*, 819–829. [[CrossRef](#)]
196. Miao, X.; Hu, Y.; Liu, J.; Wong, A. Porous calcium phosphate ceramics prepared by coating polyurethane foams with calcium phosphate cements. *Mater. Lett.* **2004**, *58*, 397–402. [[CrossRef](#)]
197. Maidaniuc, A.; Miculescu, F.; Voicu, S.I.; Andronesu, C.; Miculescu, M.; Matei, E.; Mocanu, A.C.; Pencea, I.; Csaki, I.; Machedon-Pisu, T.; et al. Induced wettability and surface-volume correlation of composition for bovine bone derived hydroxyapatite particles. *Appl. Surf. Sci.* **2018**, *438*, 158–166. [[CrossRef](#)]
198. Paital, S.R.; Dahotre, N.B. Wettability and kinetics of hydroxyapatite precipitation on a laser-textured Ca–P bioceramic coating. *Acta Biomater.* **2009**, *5*, 2763–2772. [[CrossRef](#)]
199. Bodhak, S.; Bose, S.; Bandyopadhyay, A. Role of surface charge and wettability on early stage mineralization and bone cell–materials interactions of polarized hydroxyapatite. *Acta Biomater.* **2009**, *5*, 2178–2188. [[CrossRef](#)]
200. Doshi, B.; Sillanpää, M.; Kalliola, S. A review of bio-based materials for oil spill treatment. *Water Res.* **2018**, *135*, 262–277. [[CrossRef](#)]

201. Thian, E.S.; Ahmad, Z.; Huang, J.; Edirisinghe, M.J.; Jayasinghe, S.N.; Ireland, D.C.; Brooks, R.A.; Rushton, N.; Bonfield, W.; Best, S.M. The role of surface wettability and surface charge of electrosprayed nanoapatites on the behaviour of osteoblasts. *Acta Biomater.* **2010**, *6*, 750–755. [[CrossRef](#)]
202. Aronov, D.; Rosen, R.; Ron, E.; Rosenman, G. Tunable hydroxyapatite wettability: Effect on adhesion of biological molecules. *Process. Biochem.* **2006**, *41*, 2367–2372. [[CrossRef](#)]
203. Fornell, J.; Feng, Y.; Pellicer, E.; Suriñach, S.; Baró, M.; Sort, J. Mechanical behaviour of brushite and hydroxyapatite coatings electrodeposited on newly developed FeMnSiPd alloys. *J. Alloys Compd.* **2017**, *729*, 231–239. [[CrossRef](#)]
204. Fathyunes, L.; Khalil-Allafi, J.; Moosavifar, M. Development of graphene oxide/calcium phosphate coating by pulse electrodeposition on anodized titanium: Biocorrosion and mechanical behavior. *J. Mech. Behav. Biomed. Mater.* **2018**, *90*, 575–586. [[CrossRef](#)]
205. Singh, S.; Prakash, C.; Singh, H. Deposition of HA-TiO₂ by plasma spray on β -phase Ti-35Nb-7Ta-5Zr alloy for hip stem: Characterization, mechanical properties, corrosion, and in-vitro bioactivity. *Surf. Coat. Technol.* **2020**, *398*, 126072. [[CrossRef](#)]
206. Drevet, R.; Fauré, J.; Benhayoune, H. Thermal Treatment Optimization of Electrodeposited Hydroxyapatite Coatings on Ti6Al4V Substrate. *Adv. Eng. Mater.* **2012**, *14*, 377–382. [[CrossRef](#)]
207. Harun, W.; Asri, R.; Alias, J.; Zulkifli, F.; Kadirgama, K.; Ghani, S.; Shariffuddin, J. A comprehensive review of hydroxyapatite-based coatings adhesion on metallic biomaterials. *Ceram. Int.* **2018**, *44*, 1250–1268. [[CrossRef](#)]
208. ISO 13779-4; Implants for Surgery—Hydroxyapatite—Part 4: Determination of Coating Adhesion Strength. International Organization for Standardization: Geneva, Switzerland, 2018.
209. Lei, W.-S.; Mittal, K.; Yu, Z. Adhesion Measurement of Coatings on Biodevices/Implants: A Critical Review. *Rev. Adhes. Adhes.* **2016**, *4*, 367–397. [[CrossRef](#)]
210. Kurzweg, H.; Heimann, R.B.; Troczynski, T. Adhesion of thermally sprayed hydroxyapatite–bond–coat systems measured by a novel peel test. *J. Mater. Sci. Mater. Med.* **1998**, *9*, 9–16. [[CrossRef](#)] [[PubMed](#)]
211. Barnes, D.; Johnson, S.; Snell, R.; Best, S. Using scratch testing to measure the adhesion strength of calcium phosphate coatings applied to poly(carbonate urethane) substrates. *J. Mech. Behav. Biomed. Mater.* **2011**, *6*, 128–138. [[CrossRef](#)] [[PubMed](#)]
212. Hsu, H.-C.; Wu, S.-C.; Lin, C.-Y.; Ho, W.-F. Characterization of Hydroxyapatite/Chitosan Composite Coating Obtained from Crab Shells on Low-Modulus Ti-25Nb-8Sn Alloy through Hydrothermal Treatment. *Coatings* **2023**, *13*, 228. [[CrossRef](#)]
213. Guipont, V.; Jeandin, M.; Bansard, S.; Khor, K.A.; Nivard, M.; Berthe, L.; Cuq-Lelandais, J.-P.; Boustie, M. Bond strength determination of hydroxyapatite coatings on Ti-6Al-4V substrates using the LASer Shock Adhesion Test (LASAT). *J. Biomed. Mater. Res. Part A* **2010**, *95A*, 1096–1104. [[CrossRef](#)]
214. Uskoković, V. Ion-doped hydroxyapatite: An impasse or the road to follow? *Ceram. Int.* **2020**, *46*, 11443–11465. [[CrossRef](#)]
215. Furko, M.; Balázsi, C. Morphological, Chemical, and Biological Investigation of Ionic Substituted, Pulse Current Deposited Calcium Phosphate Coatings. *Materials* **2020**, *13*, 4690. [[CrossRef](#)]
216. Ungureanu, E.; Vranceanu, D.M.; Vladescu, A.; Parau, A.C.; Tarcolea, M.; Cotrut, C.M. Effect of Doping Element and Electrolyte's pH on the Properties of Hydroxyapatite Coatings Obtained by Pulsed Galvanostatic Technique. *Coatings* **2021**, *11*, 1522. [[CrossRef](#)]
217. Panda, S.; Biswas, C.K.; Paul, S. A comprehensive review on the preparation and application of calcium hydroxyapatite: A special focus on atomic doping methods for bone tissue engineering. *Ceram. Int.* **2021**, *47*, 28122–28144. [[CrossRef](#)]
218. Schatkoski, V.M.; do Amaral Montanheiro, T.L.; de Menezes, B.R.C.; Pereira, R.M.; Rodrigues, K.F.; Ribas, R.G.; da Silva, D.M.; Thim, G.P. Current advances concerning the most cited metal ions doped bioceramics and silicate-based bioactive glasses for bone tissue engineering. *Ceram. Int.* **2021**, *47*, 2999–3012. [[CrossRef](#)]
219. Boanini, E.; Gazzano, M.; Bigi, A. Ionic substitutions in calcium phosphates synthesized at low temperature. *Acta Biomater.* **2010**, *6*, 1882–1894. [[CrossRef](#)]
220. Bigi, A.; Boanini, E.; Gazzano, M. Ion substitution in biological and synthetic apatites. In *Biomaterialization and Biomaterials, Fundamentals and Applications*, 1st ed.; Aparicio, C., Ginebra, M.P., Eds.; Woodhead Publishing (Elsevier): Sawston, UK, 2015; pp. 235–266. ISBN 9781782423386.
221. Wang, W.; Yeung, K.W.K. Bone grafts and biomaterials substitutes for bone defect repair: A review. *Bioact. Mater.* **2017**, *2*, 224–247. [[CrossRef](#)]
222. Arcos, D.; Vallet-Regí, M. Substituted hydroxyapatite coatings of bone implants. *J. Mater. Chem. B* **2020**, *8*, 1781–1800. [[CrossRef](#)]
223. Ratnayake, J.T.B.; Mucalo, M.; Dias, G.J. Substituted hydroxyapatites for bone regeneration: A review of current trends. *J. Biomed. Mater. Res. Part B Appl. Biomater.* **2016**, *105*, 1285–1299. [[CrossRef](#)]
224. Dubnika, A.; Loca, D.; Rudovica, V.; Parekh, M.B.; Berzina-Cimdina, L. Functionalized silver doped hydroxyapatite scaffolds for controlled simultaneous silver ion and drug delivery. *Ceram. Int.* **2017**, *43*, 3698–3705. [[CrossRef](#)]
225. Chen, K.; Ustriyana, P.; Moore, F.; Sahai, N. Biological Response of and Blood Plasma Protein Adsorption on Silver-Doped Hydroxyapatite. *ACS Biomater. Sci. Eng.* **2019**, *5*, 561–571. [[CrossRef](#)]
226. Mokabber, T.; Cao, H.; Norouzi, N.; Van Rijn, P.; Pei, Y. Antimicrobial Electrodeposited Silver-Containing Calcium Phosphate Coatings. *ACS Appl. Mater. Interfaces* **2020**, *12*, 5531–5541. [[CrossRef](#)]
227. Wiesmann, H.-P.; Plate, U.; Zierold, K.; Hohling, H.J. Potassium is Involved in Apatite Biomineralization. *J. Dent. Res.* **1998**, *77*, 1654–1657. [[CrossRef](#)]
228. Kannan, S.; Ventura, J.; Ferreira, J. Synthesis and thermal stability of potassium substituted hydroxyapatites and hydroxyapatite/ β -tricalciumphosphate mixtures. *Ceram. Int.* **2007**, *33*, 1489–1494. [[CrossRef](#)]

229. Kumar, M.; Xie, J.; Chittur, K.; Riley, C. Transformation of modified brushite to hydroxyapatite in aqueous solution: Effects of potassium substitution. *Biomaterials* **1999**, *20*, 1389–1399. [[CrossRef](#)]
230. Kaygili, O.; Keser, S.; Ates, T.; Yakuphanoglu, F. Synthesis and characterization of lithium calcium phosphate ceramics. *Ceram. Int.* **2013**, *39*, 7779–7785. [[CrossRef](#)]
231. Pan, C.; Chen, L.; Wu, R.; Shan, H.; Zhou, Z.; Lin, Y.; Yu, X.; Yan, L.; Wu, C. Lithium-containing biomaterials inhibit osteoclastogenesis of macrophages in vitro and osteolysis in vivo. *J. Mater. Chem. B* **2018**, *6*, 8115–8126. [[CrossRef](#)] [[PubMed](#)]
232. Wang, Y.; Yang, X.; Gu, Z.; Qin, H.; Li, L.; Liu, J.; Yu, X. In vitro study on the degradation of lithium-doped hydroxyapatite for bone tissue engineering scaffold. *Mater. Sci. Eng. C* **2016**, *66*, 185–192. [[CrossRef](#)] [[PubMed](#)]
233. Li, H.; Zhao, X.; Cao, S.; Li, K.; Chen, M.; Xu, Z.; Lu, J.; Zhang, L. Na-doped hydroxyapatite coating on carbon/carbon composites: Preparation, in vitro bioactivity and biocompatibility. *Appl. Surf. Sci.* **2012**, *263*, 163–173. [[CrossRef](#)]
234. Kannan, S.; Ventura, J.M.G.; Lemos, A.F.; Barba, A.; Ferreira, J.M.F. Effect of sodium addition on the preparation of hydroxyapatites and biphasic ceramics. *Ceram. Int.* **2008**, *34*, 7–13. [[CrossRef](#)]
235. Cho, J.S.; Um, S.-H.; Yoo, D.S.; Chung, Y.-C.; Chung, S.H.; Lee, J.-C.; Rhee, S.-H. Enhanced osteoconductivity of sodium-substituted hydroxyapatite by system instability. *J. Biomed. Mater. Res. Part B Appl. Biomater.* **2013**, *102*, 1046–1062. [[CrossRef](#)]
236. Tang, C.-M.; Fan, F.-Y.; Ke, Y.-C.; Lin, W.-C. Effects of electrode plate annealing treatment and the addition of hydrogen peroxide on improving the degradation of cobalt hydroxyapatite for bone repair. *Mater. Chem. Phys.* **2020**, *259*, 123962. [[CrossRef](#)]
237. Lin, W.-C.; Chuang, C.-C.; Wang, P.-T.; Tang, C.-M. A Comparative Study on the Direct and Pulsed Current Electrodeposition of Cobalt-Substituted Hydroxyapatite for Magnetic Resonance Imaging Application. *Materials* **2018**, *12*, 116. [[CrossRef](#)]
238. Drevet, R.; Zhukova, Y.; Dubinskiy, S.; Kazakbiev, A.; Naumenko, V.; Abakumov, M.; Fauré, J.; Benhayoune, H.; Prokoshkin, S. Electrodeposition of cobalt-substituted calcium phosphate coatings on Ti22Nb6Zr alloy for bone implant applications. *J. Alloys Compd.* **2019**, *793*, 576–582. [[CrossRef](#)]
239. Grass, G.; Rensing, C.; Solioz, M. Metallic Copper as an Antimicrobial Surface. *Appl. Environ. Microbiol.* **2011**, *77*, 1541–1547. [[CrossRef](#)]
240. Wolf-Brandstetter, C.; Oswald, S.; Bierbaum, S.; Wiesmann, H.-P.; Scharnweber, D. Influence of pulse ratio on codeposition of copper species with calcium phosphate coatings on titanium by means of electrochemically assisted deposition. *J. Biomed. Mater. Res. Part B Appl. Biomater.* **2013**, *102*, 160–172. [[CrossRef](#)]
241. Prosolov, K.A.; Lastovka, V.V.; Khimich, M.A.; Chebodaeva, V.V.; Khlusov, I.A.; Sharkeev, Y.P. RF Magnetron Sputtering of Substituted Hydroxyapatite for Deposition of Biocoatings. *Materials* **2022**, *15*, 6828. [[CrossRef](#)]
242. Farzadi, A.; Bakhshi, F.; Solati-Hashjin, M.; Asadi-Eydivand, M.; abu Osman, N.A. Magnesium incorporated hydroxyapatite: Synthesis and structural properties characterization. *Ceram. Int.* **2014**, *40*, 6021–6029. [[CrossRef](#)]
243. Cacciotti, I.; Bianco, A.; Lombardi, M.; Montanaro, L. Mg-substituted hydroxyapatite nanopowders: Synthesis, thermal stability and sintering behaviour. *J. Eur. Ceram. Soc.* **2009**, *29*, 2969–2978. [[CrossRef](#)]
244. Vranceanu, D.M.; Ionescu, I.C.; Ungureanu, E.; Cojocaru, M.O.; Vladescu, A.; Cotrut, C.M. Magnesium Doped Hydroxyapatite-Based Coatings Obtained by Pulsed Galvanostatic Electrochemical Deposition with Adjustable Electrochemical Behavior. *Coatings* **2020**, *10*, 727. [[CrossRef](#)]
245. Huang, Y.; Qiao, H.; Nian, X.; Zhang, X.; Zhang, X.; Song, G.; Xu, Z.; Zhang, H.; Han, S. Improving the bioactivity and corrosion resistance properties of electrodeposited hydroxyapatite coating by dual doping of bivalent strontium and manganese ion. *Surf. Coat. Technol.* **2016**, *291*, 205–215. [[CrossRef](#)]
246. Huang, Y.; Ding, Q.; Han, S.; Yan, Y.; Pang, X. Characterisation, corrosion resistance and in vitro bioactivity of manganese-doped hydroxyapatite films electrodeposited on titanium. *J. Mater. Sci. Mater. Med.* **2013**, *24*, 1853–1864. [[CrossRef](#)]
247. Fadeeva, I.V.; Kalita, V.I.; Komlev, D.I.; Radiuk, A.A.; Fomin, A.S.; Davidova, G.A.; Fursova, N.K.; Murzakhonov, F.F.; Gafurov, M.R.; Fosca, M.; et al. In Vitro Properties of Manganese-Substituted Tricalcium Phosphate Coatings for Titanium Biomedical Implants Deposited by Arc Plasma. *Materials* **2020**, *13*, 4411. [[CrossRef](#)]
248. Pilmane, M.; Salma-Ancane, K.; Loca, D.; Locs, J.; Berzina-Cimdina, L. Strontium and strontium ranelate: Historical review of some of their functions. *Mater. Sci. Eng. C* **2017**, *78*, 1222–1230. [[CrossRef](#)]
249. Boanini, E.; Torricelli, P.; Fini, M.; Bigi, A. Osteopenic bone cell response to strontium-substituted hydroxyapatite. *J. Mater. Sci. Mater. Med.* **2011**, *22*, 2079–2088. [[CrossRef](#)]
250. Drevet, R.; Benhayoune, H. Pulsed electrodeposition for the synthesis of strontium-substituted calcium phosphate coatings with improved dissolution properties. *Mater. Sci. Eng. C* **2013**, *33*, 4260–4265. [[CrossRef](#)]
251. Capuccini, C.; Torricelli, P.; Sima, F.; Boanini, E.; Ristoscu, C.; Bracci, B.; Socol, G.; Fini, M.; Mihailescu, I.; Bigi, A. Strontium-substituted hydroxyapatite coatings synthesized by pulsed-laser deposition: In vitro osteoblast and osteoclast response. *Acta Biomater.* **2008**, *4*, 1885–1893. [[CrossRef](#)] [[PubMed](#)]
252. Tang, Y.; Chappell, H.F.; Dove, M.T.; Reeder, R.J.; Lee, Y.J. Zinc incorporation into hydroxylapatite. *Biomaterials* **2009**, *30*, 2864–2872. [[CrossRef](#)] [[PubMed](#)]
253. Huang, Y.; Zhang, X.; Mao, H.; Li, T.; Zhao, R.; Yan, Y.; Pang, X. Osteoblastic cell responses and antibacterial efficacy of Cu/Zn co-substituted hydroxyapatite coatings on pure titanium using electrodeposition method. *RSC Adv.* **2015**, *5*, 17076–17086. [[CrossRef](#)]
254. Furko, M.; Jiang, Y.; Wilkins, T.; Balázs, C. Development and characterization of silver and zinc doped bioceramic layer on metallic implant materials for orthopedic application. *Ceram. Int.* **2016**, *42*, 4924–4931. [[CrossRef](#)]

255. El Khouri, A.; Zegzouti, A.; Elaamrani, M.; Capitelli, F. Bismuth-substituted hydroxyapatite ceramics synthesis: Morphological, structural, vibrational and dielectric properties. *Inorg. Chem. Commun.* **2019**, *110*, 107568. [[CrossRef](#)]
256. Ciobanu, G.; Bargan, A.M.; Luca, C. New Bismuth-Substituted Hydroxyapatite Nanoparticles for Bone Tissue Engineering. *JOM* **2015**, *67*, 2534–2542. [[CrossRef](#)]
257. Ahmed, M.K.; Mansour, S.F.; Mostafa, M.S.; Darwesh, R.; El-Dek, S.I. Structural, mechanical and thermal features of Bi and Sr co-substituted hydroxyapatite. *J. Mater. Sci.* **2018**, *54*, 1977–1991. [[CrossRef](#)]
258. Lin, Y.; Yang, Z.; Cheng, J. Preparation, Characterization and Antibacterial Property of Cerium Substituted Hydroxyapatite Nanoparticles. *J. Rare Earths* **2007**, *25*, 452–456. [[CrossRef](#)]
259. Feng, Z.; Liao, Y.; Ye, M. Synthesis and structure of cerium-substituted hydroxyapatite. *J. Mater. Sci. Mater. Med.* **2005**, *16*, 417–421. [[CrossRef](#)]
260. Ciobanu, G.; Harja, M. Cerium-doped hydroxyapatite/collagen coatings on titanium for bone implants. *Ceram. Int.* **2018**, *45*, 2852–2857. [[CrossRef](#)]
261. Nisar, A.; Iqbal, S.; Rehman, M.A.U.; Mahmood, A.; Younas, M.; Hussain, S.Z.; Tayyaba, Q.; Shah, A. Study of physico-mechanical and electrical properties of cerium doped hydroxyapatite for biomedical applications. *Mater. Chem. Phys.* **2023**, *299*, 127511. [[CrossRef](#)]
262. Alshemary, A.Z.; Akram, M.; Goh, Y.-F.; Kadir, M.R.A.; Abdolahi, A.; Hussain, R. Structural characterization, optical properties and in vitro bioactivity of mesoporous erbium-doped hydroxyapatite. *J. Alloys Compd.* **2015**, *645*, 478–486. [[CrossRef](#)]
263. Neacsu, I.A.; Stoica, A.E.; Vasile, B.S.; Andronescu, E. Luminescent Hydroxyapatite Doped with Rare Earth Elements for Biomedical Applications. *Nanomaterials* **2019**, *9*, 239. [[CrossRef](#)]
264. Pham, V.-H.; Van, H.N.; Tam, P.D.; Ha, H.N.T. A novel 1540nm light emission from erbium doped hydroxyapatite/ β -tricalcium phosphate through co-precipitation method. *Mater. Lett.* **2016**, *167*, 145–147. [[CrossRef](#)]
265. Yang, P.; Quan, Z.; Li, C.; Kang, X.; Lian, H.; Lin, J. Bioactive, luminescent and mesoporous europium-doped hydroxyapatite as a drug carrier. *Biomaterials* **2008**, *29*, 4341–4347. [[CrossRef](#)]
266. Al-Kattan, A.; Santran, V.; Dufour, P.; Dexpert-Ghys, J.; Drouet, C. Novel contributions on luminescent apatite-based colloids intended for medical imaging. *J. Biomater. Appl.* **2013**, *28*, 697–707. [[CrossRef](#)]
267. Graeve, O.A.; Kanakala, R.; Madadi, A.; Williams, B.C.; Glass, K.C. Luminescence variations in hydroxyapatites doped with Eu^{2+} and Eu^{3+} ions. *Biomaterials* **2010**, *31*, 4259–4267. [[CrossRef](#)]
268. Singh, R.K.; Srivastava, M.; Prasad, N.; Awasthi, S.; Dhayalan, A.; Kannan, S. Iron doped β -Tricalcium phosphate: Synthesis, characterization, hyperthermia effect, biocompatibility and mechanical evaluation. *Mater. Sci. Eng. C* **2017**, *78*, 715–726. [[CrossRef](#)]
269. Singh, R.K.; Srivastava, M.; Prasad, N.K.; Shetty, P.H.; Kannan, S. Hyperthermia effect and antibacterial efficacy of $\text{Fe}^{3+}/\text{Co}^{2+}$ co-substitutions in $\beta\text{-Ca}_3(\text{PO}_4)_2$ for bone cancer and defect therapy. *J. Biomed. Mater. Res. Part B Appl. Biomater.* **2017**, *106*, 1317–1328. [[CrossRef](#)]
270. Predoi, D.; Iconaru, S.L.; Ciobanu, S.C.; Predoi, S.-A.; Buton, N.; Megier, C.; Beuran, M. Development of Iron-Doped Hydroxyapatite Coatings. *Coatings* **2021**, *11*, 186. [[CrossRef](#)]
271. Melnikov, P.; Teixeira, A.; Malzac, A.; Coelho, M.D.B. Gallium-containing hydroxyapatite for potential use in orthopedics. *Mater. Chem. Phys.* **2009**, *117*, 86–90. [[CrossRef](#)]
272. Korbas, M.; Rokita, E.; Meyer-Klaucke, W.; Ryzek, J. Bone tissue incorporates in vitro gallium with a local structure similar to gallium-doped brushite. *JBIC J. Biol. Inorg. Chem.* **2003**, *9*, 67–76. [[CrossRef](#)] [[PubMed](#)]
273. Mosina, M.; Siverino, C.; Stipnice, L.; Scegljovs, A.; Vasiljevs, R.; Moriarty, T.F.; Locs, J. Gallium-Doped Hydroxyapatite Shows Antibacterial Activity against *Pseudomonas aeruginosa* without Affecting Cell Metabolic Activity. *J. Funct. Biomater.* **2023**, *14*, 51. [[CrossRef](#)] [[PubMed](#)]
274. Paduraru, A.V.; Oprea, O.; Musuc, A.M.; Vasile, B.S.; Iordache, F.; Andronescu, E. Influence of Terbium Ions and Their Concentration on the Photoluminescence Properties of Hydroxyapatite for Biomedical Applications. *Nanomaterials* **2021**, *11*, 2442. [[CrossRef](#)] [[PubMed](#)]
275. Jiménez-Flores, Y.; Suárez-Quezada, M.; Rojas-Trigos, J.B.; Lartundo-Rojas, L.; Suarez, M.; Mantilla, A. Characterization of Tb-doped hydroxyapatite for biomedical applications: Optical properties and energy band gap determination. *J. Mater. Sci.* **2017**, *52*, 9990–10000. [[CrossRef](#)]
276. Demnati, I.; Grossin, D.; Combes, C.; Parco, M.; Braceras, I.; Rey, C. A comparative physico-chemical study of chlorapatite and hydroxyapatite: From powders to plasma sprayed thin coatings. *Biomed. Mater.* **2012**, *7*, 054101. [[CrossRef](#)]
277. Navarrete-Segado, P.; Frances, C.; Tourbin, M.; Tenailleau, C.; Duployer, B.; Grossin, D. Powder bed selective laser process (sintering/melting) applied to tailored calcium phosphate-based powders. *Addit. Manuf.* **2021**, *50*, 102542. [[CrossRef](#)]
278. Ito, A.; Otsuka, Y.; Takeuchi, M.; Tanaka, H. Mechanochemical synthesis of chloroapatite and its characterization by powder X-ray diffractometry and attenuated total reflection-infrared spectroscopy. *Colloid Polym. Sci.* **2017**, *295*, 2011–2018. [[CrossRef](#)]
279. Merry, J.C.; Gibson, I.R.; Best, S.M.; Bonfield, W. Synthesis and characterization of carbonate hydroxyapatite. *J. Mater. Sci. Mater. Med.* **1998**, *9*, 779–783. [[CrossRef](#)]
280. Leilei, Z.; Hejun, L.; Kezhi, L.; Qiang, S.; Qiangang, F.; Yulei, Z.; Shoujie, L. Electrodeposition of carbonate-containing hydroxyapatite on carbon nanotubes/carbon fibers hybrid materials for tissue engineering application. *Ceram. Int.* **2015**, *41*, 4930–4935. [[CrossRef](#)]

281. Landi, E.; Celotti, G.; Logroscino, G.; Tampieri, A. Carbonated hydroxyapatite as bone substitute. *J. Eur. Ceram. Soc.* **2003**, *23*, 2931–2937. [[CrossRef](#)]
282. Ge, X.; Zhao, J.; Lu, X.; Li, Z.; Wang, K.; Ren, F.; Wang, M.; Wang, Q.; Qian, B. Controllable phase transformation of fluoridated calcium phosphate ultrathin coatings for biomedical applications. *J. Alloys Compd.* **2020**, *847*, 155920. [[CrossRef](#)]
283. Wang, J.; Chao, Y.; Wan, Q.; Zhu, Z.; Yu, H. Fluoridated hydroxyapatite coatings on titanium obtained by electrochemical deposition. *Acta Biomater.* **2009**, *5*, 1798–1807. [[CrossRef](#)]
284. Sun, J.; Wu, T.; Fan, Q.; Hu, Q.; Shi, B. Comparative study of hydroxyapatite, fluor-hydroxyapatite and Si-substituted hydroxyapatite nanoparticles on osteogenic, osteoclastic and antibacterial ability. *RSC Adv.* **2019**, *9*, 16106–16118. [[CrossRef](#)]
285. Wang, Y.; Wang, J.; Hao, H.; Cai, M.; Wang, S.; Ma, J.; Li, Y.; Mao, C.; Zhang, S. In Vitro and in Vivo Mechanism of Bone Tumor Inhibition by Selenium-Doped Bone Mineral Nanoparticles. *ACS Nano* **2016**, *10*, 9927–9937. [[CrossRef](#)]
286. Rodríguez-Valencia, C.; López-Álvarez, M.; Cochón-Cores, B.; Pereiro, I.; Serra, J.; González, P. Novel selenium-doped hydroxyapatite coatings for biomedical applications. *J. Biomed. Mater. Res. Part A* **2012**, *101*, 853–861. [[CrossRef](#)]
287. Tan, H.-W.; Mo, H.-J.; Lau, A.T.Y.; Xu, Y.-M. Selenium Species: Current Status and Potentials in Cancer Prevention and Therapy. *Int. J. Mol. Sci.* **2019**, *20*, 75. [[CrossRef](#)]
288. Casarrubios, L.; Gómez-Cerezo, N.; Sánchez-Salcedo, S.; Feito, M.; Serrano, M.; Saiz-Pardo, M.; Ortega, L.; de Pablo, D.; Díaz-Güemes, I.; Tomé, B.F.; et al. Silicon substituted hydroxyapatite/VEGF scaffolds stimulate bone regeneration in osteoporotic sheep. *Acta Biomater.* **2019**, *101*, 544–553. [[CrossRef](#)]
289. Aboudzadeh, N.; Dehghanian, C.; Shokrgozar, M.A. Effect of electrodeposition parameters and substrate on morphology of Si-HA coating. *Surf. Coat. Technol.* **2019**, *375*, 341–351. [[CrossRef](#)]
290. Dehghanian, C.; Aboudzadeh, N.; Shokrgozar, M.A. Characterization of silicon-substituted nano hydroxyapatite coating on magnesium alloy for biomaterial application. *Mater. Chem. Phys.* **2018**, *203*, 27–33. [[CrossRef](#)]
291. Graziani, G.; Boi, M.; Bianchi, M. A Review on Ionic Substitutions in Hydroxyapatite Thin Films: Towards Complete Biomimeticism. *Coatings* **2018**, *8*, 269. [[CrossRef](#)]
292. Mumith, A.; Cheong, V.S.; Fromme, P.; Coathup, M.J.; Blunn, G.W. The effect of strontium and silicon substituted hydroxyapatite electrochemical coatings on bone ingrowth and osseointegration of selective laser sintered porous metal implants. *PLoS ONE* **2020**, *15*, e0227232. [[CrossRef](#)] [[PubMed](#)]
293. Robinson, L.; Salma-Ancane, K.; Stipniece, L.; Meenan, B.J.; Boyd, A.R. The deposition of strontium and zinc Co-substituted hydroxyapatite coatings. *J. Mater. Sci. Mater. Med.* **2017**, *28*, 51. [[CrossRef](#)]
294. Wolf-Brandstetter, C.; Beutner, R.; Hess, R.; Bierbaum, S.; Wagner, K.; Scharnweber, D.; Gbureck, U.; Moseke, C. Multifunctional calcium phosphate based coatings on titanium implants with integrated trace elements. *Biomed. Mater.* **2020**, *15*, 025006. [[CrossRef](#)] [[PubMed](#)]
295. Liu, S.-J.; Li, H.-J.; Zhang, L.-L.; Feng, L.; Yao, P. Strontium and magnesium substituted dicalcium phosphate dehydrate coating for carbon/carbon composites prepared by pulsed electrodeposition. *Appl. Surf. Sci.* **2015**, *359*, 288–292. [[CrossRef](#)]
296. Kolmas, J.; Groszyk, E.; Kwiatkowska-Różycka, D. Substituted Hydroxyapatites with Antibacterial Properties. *BioMed Res. Int.* **2014**, *2014*, 178123. [[CrossRef](#)]
297. Garbo, C.; Locs, J.; D'Este, M.; Demazeau, G.; Mocanu, A.; Roman, C.; Horovitz, O.; Tomoaia-Cotisel, M. Advanced Mg, Zn, Sr, Si Multi-Substituted Hydroxyapatites for Bone Regeneration. *Int. J. Nanomed.* **2020**, *15*, 1037–1058. [[CrossRef](#)]
298. Bracci, B.; Torricelli, P.; Panzavolta, S.; Boanini, E.; Giardino, R.; Bigi, A. Effect of Mg^{2+} , Sr^{2+} , and Mn^{2+} on the chemico-physical and in vitro biological properties of calcium phosphate biomimetic coatings. *J. Inorg. Biochem.* **2009**, *103*, 1666–1674. [[CrossRef](#)]
299. Furko, M.; Jiang, Y.; Wilkins, T.; Balázsi, C. Electrochemical and morphological investigation of silver and zinc modified calcium phosphate bioceramic coatings on metallic implant materials. *Mater. Sci. Eng. C* **2016**, *62*, 249–259. [[CrossRef](#)]
300. Furko, M.; May, Z.; Havasi, V.; Kónya, Z.; Grünwald, A.; Detsch, R.; Boccaccini, A.R.; Balázsi, C. Pulse electrodeposition and characterization of non-continuous, multi-element-doped hydroxyapatite bioceramic coatings. *J. Solid State Electrochem.* **2017**, *22*, 555–566. [[CrossRef](#)]
301. Furko, M.; Della Bella, E.; Fini, M.; Balázsi, C. Corrosion and biocompatibility examination of multi-element modified calcium phosphate bioceramic layers. *Mater. Sci. Eng. C* **2019**, *95*, 381–388. [[CrossRef](#)]
302. Huang, Y.; Ding, Q.; Pang, X.; Han, S.; Yan, Y. Corrosion behavior and biocompatibility of strontium and fluorine co-doped electrodeposited hydroxyapatite coatings. *Appl. Surf. Sci.* **2013**, *282*, 456–462. [[CrossRef](#)]
303. Bir, F.; Khireddine, H.; Mekhalif, Z.; Bonnamy, S. Pulsed electrodeposition of Ag^+ doped prosthetic Fluorohydroxyapatite coatings on stainless steel substrates. *Mater. Sci. Eng. C* **2020**, *118*, 111325. [[CrossRef](#)]
304. Vo, T.H.; Le, T.D.; Pham, T.N.; Nguyen, T.T.; Nguyen, T.P.; Dinh, T.M.T. Electrodeposition and characterization of hydroxyapatite coatings doped by Sr^{2+} , Mg^{2+} , Na^+ and F^- on 316L stainless steel. *Adv. Nat. Sci. Nanosci. Nanotechnol.* **2018**, *9*, 045001. [[CrossRef](#)]
305. Chambard, M.; Remache, D.; Balcaen, Y.; Dalverny, O.; Alexis, J.; Siadous, R.; Bareille, R.; Catros, S.; Fort, P.; Grossin, D.; et al. Effect of silver and strontium incorporation route on hydroxyapatite coatings elaborated by rf-SPS. *Materialia* **2020**, *12*, 100809. [[CrossRef](#)]

Disclaimer/Publisher's Note: The statements, opinions and data contained in all publications are solely those of the individual author(s) and contributor(s) and not of MDPI and/or the editor(s). MDPI and/or the editor(s) disclaim responsibility for any injury to people or property resulting from any ideas, methods, instructions or products referred to in the content.